Hindawi
Journal of Advanced Transportation
Volume 2020, Article ID 6301703, 21 pages
https://doi.org/10.1155/2020/6301703

Research Article

Vehicle Movement Analyses Considering Altitude Based on Modified Digital Elevation Model and Spherical Bilinear Interpolation Model: Evidence from GPS-Equipped Taxi Data in Sanya, Zhengzhou, and Liaoyang

Jiawei Gui [1,2] **and Qunqi Wu** [1,2]

[1]*School of Economics and Management, Chang'an University, Xi'an, Shanxi 710064, China*
[2]*Center of Comprehensive Transportation Economic Management, Chang'an University, Xi'an, Shanxi 710064, China*

Correspondence should be addressed to Jiawei Gui; gjw@chd.edu.cn

Received 25 May 2019; Revised 13 October 2019; Accepted 28 October 2019; Published 20 January 2020

Guest Editor: Kamal D. Singh

Aggravating energy shortages and increasing labor costs have become global problems and have garnered special importance in recent years in the transportation sector, especially in taxi markets. Automatic vehicles have a bright future, however, there is an equal amount of skepticism and concern about safety for all the optimism. To unlock the potential of automatic vehicles in intelligent transportation systems, a lot more data and testing are required to promote safety level as far as possible and achieve the organizational aim of reducing accidents to zero tolerance. And it is vital to provide accurate models for vehicle movement analyses. In this study, Modified Digital Elevation (MDE) model and Spherical Bilinear Interpolation (SBI) model were proposed for vehicle movement analyses considering altitude. And the experimental data of 9,990 GPS-enabled taxis in Sanya, Zhengzhou, and Liaoyang were adopted to support comparisons. Measurement results showed that MDE model had over 99% less disparity with direct solution than original model and SBI model could further improve the effects. It indicated that the application of MDE model and SBI model could improve both accuracy and efficiency of vehicle movement analyses and it had a bright future in the field of automatic vehicles. Future directions could be improving models and expanding data.

1. Introduction

Nowadays, there are plenty of urgent social issues in the transportation research field. For example, aggravating energy shortages and increasing labor costs have become global problems and have garnered special importance in recent years in the transportation sector, especially in taxi markets. With the worsening situation of energy shortages and labor costs, taxi markets are facing increasing opportunities as well as challenges. It is essential that appropriate counter measures must be taken to suppress or reverse or at least alleviate the worsening situation.

With the rapid progress of self-driving technologies, there are more and more advanced applications involved in intelligent traffic system. For example, automatic vehicles have a bright future. Dubai Roads and Transportation Authority tested autonomous pods, the world's first automatic taxi, in 2018. According to the evidence lab of union bank of Switzerland, the number of taxis in New York might drop by two-thirds if automatic vehicles were promoted completely, and the global automatic taxi market may exceed $2 trillion by 2030. Tesla Inc published a full self-driving computer called Autopilot 3.0 and an automatic taxi plan called Robo Taxi. Besides, many companies have already tested their automatic taxis or automatic buses along the road, such as Waymo in USA, Yandex in Russia, Gateway in UK, Easymile in France, Bestmile in Switzerland, Vislab in Italia, ZMP in Japan, KT in South Korea, GAC in China, etc.

However, there is an equal amount of skepticism and concern for all the optimism surrounding automatic vehicles. Most crucially, many people doubt the safety of automatic vehicles because they are not controlled by reliable human

drivers but computers. On March 19th in 2018, a terrible accident took place in Tempe, Arizona that a 49-year-old woman with a bicycle on the sidewalk was hit to die by an Uber self-driving car at a speed of 65 kilometers per hour. Since then, the willingness of the public to ride in a fully self-driving vehicle fell in a very low level.

To unlock the potential of automatic vehicles in intelligent transportation systems, a lot more data and testing are required to promote safety level as far as possible and achieve the organizational aim of reducing accidents to zero tolerance. And it is vital to provide accurate models for vehicle movement analyses. In this study, modified digital elevation model and spherical bilinear interpolation model were proposed for vehicle movement analyses considering altitude. And GPS-enabled taxi data in Sanya, Zhengzhou, and Liaoyang were adopted to support comparisons.

The rest of this paper were organized as follows: Section 2 reviewed related works; Section 3 introduced formulas, models, data and tools; Section 4 presented a sample and described results in Sanya, Zhengzhou, and Liaoyang; Section 5 made a discussion; Section 6 summarized main conclusions, contributions and proposed future directions.

2. Literature Review

In this section, there are several similar problems and some related works till date, including Internet of Vehicles problem (see Section 2.1), data analysis for automatic vehicles (see Section 2.2) and taxi service improving problem (see Section 2.3).

2.1. Internet of Vehicles Problem. The Internet is a popular network technology all over the world and it has continuous developments in recent years. The evolution of network technology has led to a deployment of various access networks as introduced by Piamrat et al. [1]. Internet of Things (IoT) is a novel paradigm that is rapidly gaining ground in the scenario of modern wireless telecommunications as addressed by Atzori et al. [2]. Miorandi et al. proposed an overview of IoT technologies and services [3]. Xu et al. reviewed classical researches of IoT technologies and major applications in industries [4]. Zanella et al. proposed an urban IoT system and explored the application of the IoT paradigm to smart cities, taking Padova of Italy as an example [5].

Intelligent Transportation Systems (ITS) had significant impact on our life as introduced by Wang [6]. Internet of Vehicle (IoV) is one of the revolutions mobilized by IoT as addressed by Kaiwartya et al. [7]. Lu et al. regarded IoV as the next frontier for automotive revolution and the key to the evolution to ITS [8]. Yang et al. proposed an abstract network model of the IoV and presented its applications [9]. However, IoV also posed new challenges to the communication technology [10]. The information security of IoV was a considerable challenge. Singh et al. presented the potential of transforming vehicle communication in terms of efficiency and safety [11]. Chen proposed a trust-based cooperation authentication bit-map routing protocol against insider security threats in wireless ad-hoc networks [12]. Huang et al. proposed a proactive scheme to secure Edge computing-based IoV against RSU hotspot attack [13]. Furthermore, IoV has rapid developments in recent years. Butt et al. presented a scalable Social IoV (SIoV) architecture based on Restful web technology [14]. Chen et al. proposed Cognitive IoV (CIoV) to enhance transportation safety and network security by communication technologies [15].

Vehicular Ad-hoc Networks (VANET) comprise communications among vehicles and infrastructures by wireless local network technologies as addressed by Hartenstein and Laberteaux [16]. With the wide spread of Global Positioning System (GPS) and Geographic Information System (GIS), the participants in VANET could acquire much more information than before. Benefit from that, GPS-Equipped cars could not only acquire their real-time locations, but also road directions. Thus, VANET technologies helped improving road safety and providing comfort for passengers [17, 18]. In the field of ITS, IoV and VANET technologies created essential conditions for automatic vehicles.

2.2. Data Analysis for Automatic Vehicles. Automatic vehicles are regarded as the future of transportation. It has been a long-lasting dream of robotics researchers and enthusiasts as indicated by Petrovskaya and Thrun [19]. However, safety is the dominant factor in any automatic vehicle control system design as proposed by Shladover et al. [20]. Much more work was required until autonomous vehicles could participate in real-world urban traffic safely and robustly as proposed by Luettel et al. [21]. To ensure the safety of autonomous vehicles, a holistic fleet deployment scheme from interdisciplinary perspectives should be established as proposed by Koopman and Wagner [22]. Wang et al. investigated the acceptance of intelligent driving vehicles in Guangzhou and indicated that consumers focused on not only the developmental prospects but also the technological safety of intelligent driving vehicles [23]. With the rapid progress of IoV and VANET, there is a great deal of technologies involved in data analysis for automatic vehicles, which are described as follows.

(i) Vehicle communication systems. Machine-to-Machine (M2M) communication for the IoT system was considered to be a key technology in future networks as introduced by Chen et al. [24]. Park et al. proposed a transmission strategy for use with a capillary M2M system under wireless personal area networks based on a series of performance analysis for contention adaptation of M2M devices with directional antennas [25, 26]. Zhou et al. proposed a two-stage access control and resource allocation algorithm based on M2M communication and verified it under various simulation scenarios. With the rapid progress of IoV and VANET, M2M communication has been applied to vehicle communication in recent years. The vehicle communication systems include but are not limited to Vehicle-to-Pedestrian (V2P), Vehicle-to-Vehicle (V2V) and Vehicle-to-Infrastructure (V2I). Rahimian et al. examined the feasibility that sending traffic warnings to texting pedestrians based on V2P communication when they initiate an unsafe road crossing influences their decisions and actions [27]. Fan et al. proposed a traffic-aware relay selection based on millimeter-wave

V2V communication to overcome the Line-of-sight blockage problem [28]. Lyamin et al. proposed a data-mining-based method for V2V communications by random and On-off models [26]. Han et al. proposed an optimal signal control algorithm for signalized intersections using individual vehicle's trajectory data based on V2I communication [30]. Jia et al. verified that autonomous vehicles have significantly improvements on traffic efficiency via V2V and V2I communications [31].

(ii) Machine learning methods. Machine learning were used to identify objects in images, transcribe speech into text, match news items, posts or products with users' interests, and select relevant results of search as introduced by Lecun et al. [32]. With the rapid progress of IoV and VANET, machine learning methods has been applied to vehicle simulation, emulation and prediction in recent years. Aramrattana et al. proposed a simulation framework for cooperative safety assessment and efficiency evaluation in ITS [33]. Elwekeil et al. proposed a deep learning approach to achieve both reliability and spectrum efficiency of V2V communications [34]. Lv et al. proposed a modified cyber-physical system for automated electric vehicles based on unsupervised machine learning algorithms [35]. Li et al. proposed a proactively load balancing approach for vehicular network traffic control based on V2I communication, convolutional neural networks and deep learning to enable efficient cooperation among mobile edge servers [36].

(iii) Big data technologies. In recent years, a significant change in ITS was that much more data were collected from a variety of sources and can be processed into various forms as proposed by Zhang et al. [37]. And numerous advanced multidisciplinary journals began publishing a special issue of big data, for instance, Nature in 2008 [38] and Science in 2011 [39]. To solve big data, several technologies were proposed, including cloud computing, artificial intelligence and blockchain technology. Gubbi et al. proposed a cloud centric vision for worldwide implementation of IoT [40]. Whaiduzzaman et al. verified that cloud computing was a technologically feasible and economically viable paradigm for vehicles [41]. Al-Fuqaha et al. explored the relationships between IoT and big data analytics [42]. Ning et al. proposed a three-layer model based on fog computing to enable distributed traffic management and verified it by trajectory-based performance analysis [43]. As for applications, more and more researches focus on large scale taxi GPS data [44–46].

2.3. Taxi Service Improving Problem. Taxi is the main constituent of urban transportation. With the rapid progress of wireless sensor network [47], vehicle markets meet an evolution from intelligent vehicle grid to autonomous, Internet-connected vehicles and vehicular cloud as discussed by Gerla et al. [48]. Automatic taxis have gradually become reality in several advanced regions but not fully promoted yet. Just like every coin has two sides, automatic taxis have advantages and disadvantages. On the one hand, automatic taxis overcome some defects of human drivers, including excessive stress [49], inadequate sleepiness [50], and negative behaviors [51]. On the other hand, automatic taxis need mountains of work to achieve functions and ensure security. Taxi automation is one of the most promising technologies for the future and it is a challenge well worth meeting for taxi companies.

Fast and reliable service that can compete with the single occupancy vehicle was one of the demands of transit users as proposed by El-Geneidy et al. [52]. And it has become significant to provide users with a range of security-related and user-oriented vehicular applications as proposed by Ning et al. [53]. Thus, it is necessary for taxi companies improve their service to meet the demand of passengers. Yuan et al. proposed a price equilibrium model for taxi market to improve the service level [54]. Song et al. proposed a planning concept from the perspective of supply and demand economic equilibrium to optimize the transportation markets [55]. Dou et al. proposed a heuristic line piloting method that a taxi deviating from the typical route would raise an alert when malfunction took place or even hijacked by criminals [56]. Tang et al. proposed a customer-search model based on route choice behavior analysis to help taxi drivers find next passengers in urban road networks [57]. Although taxi companies and governments have already made great efforts, there are still plenty of service improving problems to be settled.

To unlock the potential of IoV in ITS, in the previous study [58], Gui and Wu measured taxi efficiency based on 2191 GPS-equipped taxi data in Sanya and indicated that the application of Motorcade-Sharing model could not only alleviate urban traffic congestion but also optimize urban taxi markets. However, altitude was not considered in that study which might reduce the measurement accuracy and result in lower safety level when altitude is nonnegligible. Thus, Original Model need improvements.

To sum up, some helpful works have already been done. However, few researches took altitude into consideration and proposed accurate models for vehicle movement analyses. Besides, autonomous vehicles need assigning continuous directives in time while it is difficult for complex algorithms to response immediately under the background of big data.

How much the altitude will affect the vehicle movement analyses? How to simplify complex algorithms of the Direct Solution for automatic vehicles? And how to handle the situation when some data was missing? In the next section, methods and data are involved to explore these questions.

3. Methods and Materials

In this section, there are several parts of methods and materials. First, an analysis procedure was presented as an overview (see Section 3.1). Second, traditional methods were reviewed, including Direct Solution (see Section 3.2) and Original Model (see Section 3.3). Third, modified models were proposed, including MDE model (see Section 3.4) and SBI model (see Section 3.5).

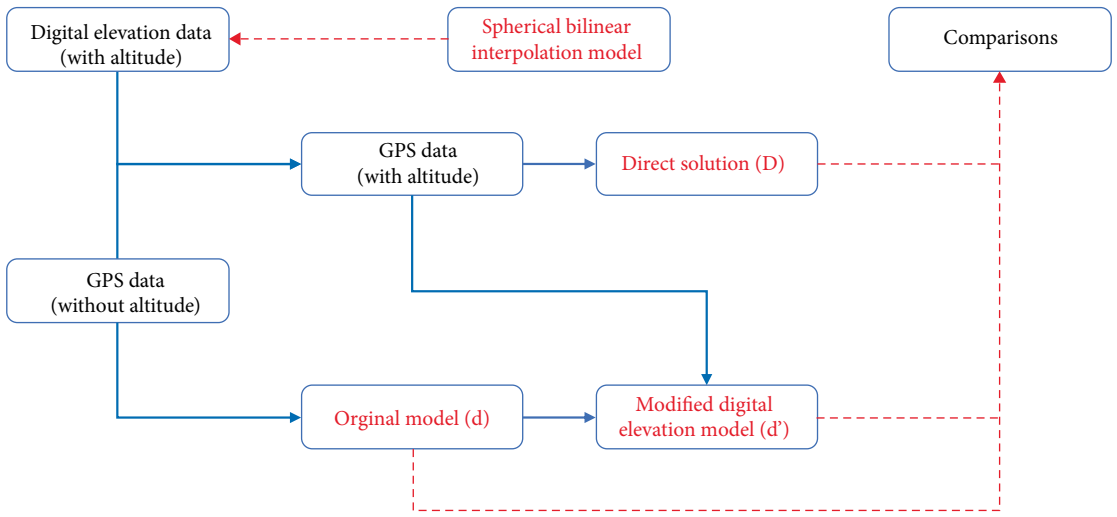

Figure 1: Analysis procedure design.

Table 1: Function comparison of direct solution, original model, and MDE model.

Data source	Data	Direct solution (D)	Original model (d)	MDE model (d')
GPS data (without altitude)	Longitude	√	√	√
	Latitude	√	√	√
Digital elevation data	Altitude	√		√

3.1. Analysis Procedure. To solve this problem, a series of analysis procedure was established (see Figure 1).

In terms of data, GPS data without altitude and digital elevation data were collected at the beginning. GPS data with altitude was calculated on the basis of them afterwards (see Section 3.6). And the preciseness of GPS data with altitude was further improved by Spherical Bilinear Interpolation (SBI) Model (see Section 3.5).

In terms of model, three models were adopted for analyzing vehicle movements. They are direct solution (see Section 3.2), original model (see Section 3.3) and Modified Digital Elevation (MDE) model (see Section 3.4) and they have different functions (see Table 1).

(i) Direct solution. It is the traditional approach with large computation requirements because of its square algorithm, which is one of its drawbacks.

(ii) Original model. It simplifies the square algorithm of Direct Solution by cosine theorems (see Distance Formula in the previous study [58]). However, it ignores altitude which affects the measurement accuracy of results when altitude is nonnegligible.

(iii) MDE model. It adopts original model and takes altitude into consideration. In theory, MDE model has more accurate results than original model especially when altitude is nonnegligible. In addition, MDE model adopts SBI model to improve the preciseness of GPS data with altitude.

In this study, vehicle movements were analyzed by 3 models above mentioned at the same time and then a series of comparisons were raised on the basis of results. The notations for variables were in the Appendix (see Appendix A).

3.2. Direct Solution. Direct solution is the traditional approach and it calculates distances in a direct way (see Figure 2).

There are 4 steps in this section.

First, in order to describe the location of vehicles in a mathematical way, the Spherical Coordinate System was established in Formula (1).

$$P(\rho, \theta, \varphi), \tag{1}$$

where $\rho \geq 0, 0 \leq \theta \leq \pi$, and $0 \leq \varphi < 2\pi$. The variable ρ represents the radial distance. The variable θ represents the polar angle. The variable φ represents the azimuthal angle. The radial distance can be divided into two parts by Formula (2).

$$\rho = R + h, \tag{2}$$

where $R = 6378137.00$ (m), which represents the radius of the earth. The variable h represents the altitude. Based on Formulas (1), (2), the coordinate of vector $\overrightarrow{OP}$ in Spherical Coordinate System can be represented by Formula (3).

$$\overrightarrow{OP} = (R + h, \theta, \varphi). \tag{3}$$

Second, in order to calculate the distance between two locations by Distance Formula, the Rectangular Coordinate System was established in Formula (4).

$$\overrightarrow{OP} = (x, y, z). \tag{4}$$

Based on Distance Formula, the distance between points P_1 and P_2 in Rectangular Coordinate System can be calculated by Formula (5).

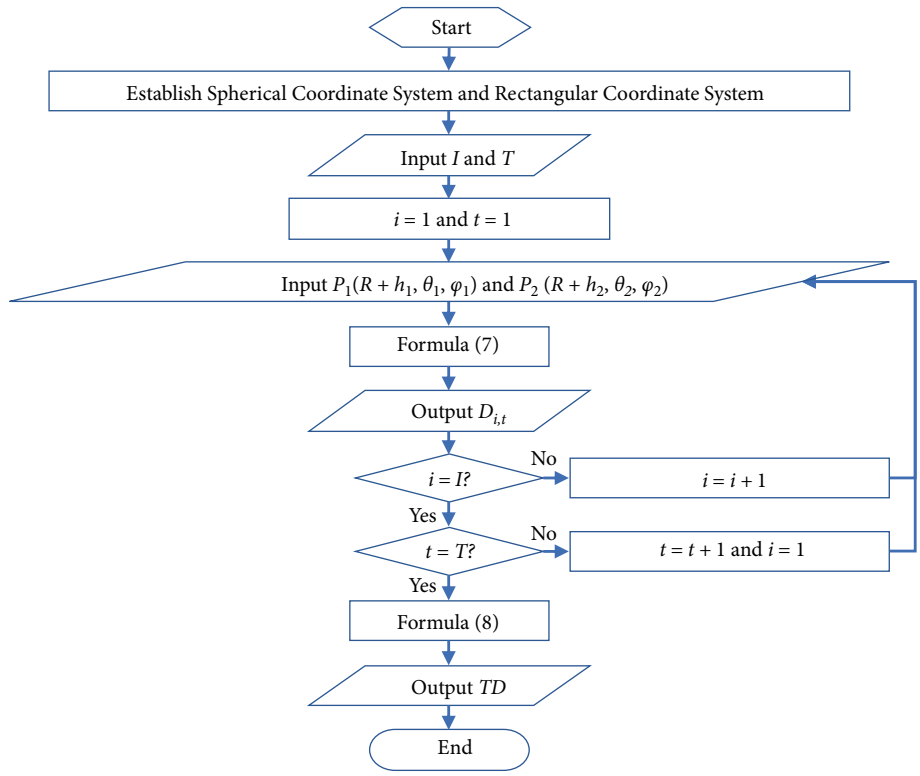

Figure 2: Flow chart of direct solution.

$$|P_1P_2| = \sqrt{(\Delta x)^2 + (\Delta y)^2 + (\Delta z)^2}. \tag{5}$$

Third, spherical coordinates were converted into rectangular coordinates. Based on Formulas (1), (4), the relationship of them can be represented by Formula (6).

$$\begin{aligned} x &= \rho \sin\theta \cos\varphi, \\ y &= \rho \sin\theta \sin\varphi, \\ z &= \rho \cos\theta. \end{aligned} \tag{6}$$

Based on Formula (6), the spherical coordinate of point $P_1(R + h_1, \theta_1, \varphi_1)$ was converted into $P_1((R + h_1)\sin\theta_1 \cos\varphi_1, (R + h_1)\sin\theta_1 \sin\varphi_1, (R + h_1)\cos\theta_1)$ in Rectangular Coordinate System, and the spherical coordinate of point $P_2(R + h_2, \theta_2, \varphi_2)$ was converted into $P_2((R + h_2)\sin\theta_2 \cos\varphi_2, (R + h_2)\sin\theta_2 \sin\varphi_2, (R + h_2)\cos\theta_2)$ in Rectangular Coordinate System.

Based on Formula (5), the distance between points P_1 and P_2 under direct solution can be calculated by Formula (7), which was sophisticated to some extent.

$$D = \sqrt{\left[(R + h_1)\sin\theta_1 \cos\varphi_1 - (R + h_2)\sin\theta_2 \cos\varphi_2\right]^2 + \left[(R + h_1)\sin\theta_1 \sin\varphi_1 - (R + h_2)\sin\theta_2 \sin\varphi_2\right]^2 + \left[(R + h_1)\cos\theta_1 - (R + h_2)\cos\theta_2\right]^2}. \tag{7}$$

Fourth, all the distances were summed up. Supposing that the variable TD represents total movements of vehicles under Direct Solution and it can be calculated by Formula (8).

$$TD = \sum_{i=1}^{I} \sum_{t=1}^{T} D_{i,t}. \tag{8}$$

3.3. Original Model. Original Model simplifies the square algorithm of Direct Solution by cosine theorems and it calculates distances in a simple way (see Figure 3).

There are 5 steps in this section.

First, the Spherical Coordinate System was established in Formula (1).

Second, the Rectangular Coordinate System was established in Formula (4).

Third, in order to calculate the distance between two locations, the cosine value of the angle between vectors $\overrightarrow{OP_1}$ and $\overrightarrow{OP_2}$ was calculated by Formula (9).

$$\cos\left\langle \overrightarrow{OP_1}, \overrightarrow{OP_2} \right\rangle = \frac{\overrightarrow{OP_1} \cdot \overrightarrow{OP_2}}{\left|\overrightarrow{OP_1}\right|\left|\overrightarrow{OP_2}\right|}. \tag{9}$$

Formula (9) can be converted into Formula (10) and the derivation process is in the Appendix part (see Appendix B in the previous study [58]).

$$\cos\left\langle \overrightarrow{OP_1}, \overrightarrow{OP_2} \right\rangle = \sin\theta_1 \sin\theta_2 \cos(\varphi_2 - \varphi_1) + \cos\theta_1 \cos\theta_2. \tag{10}$$

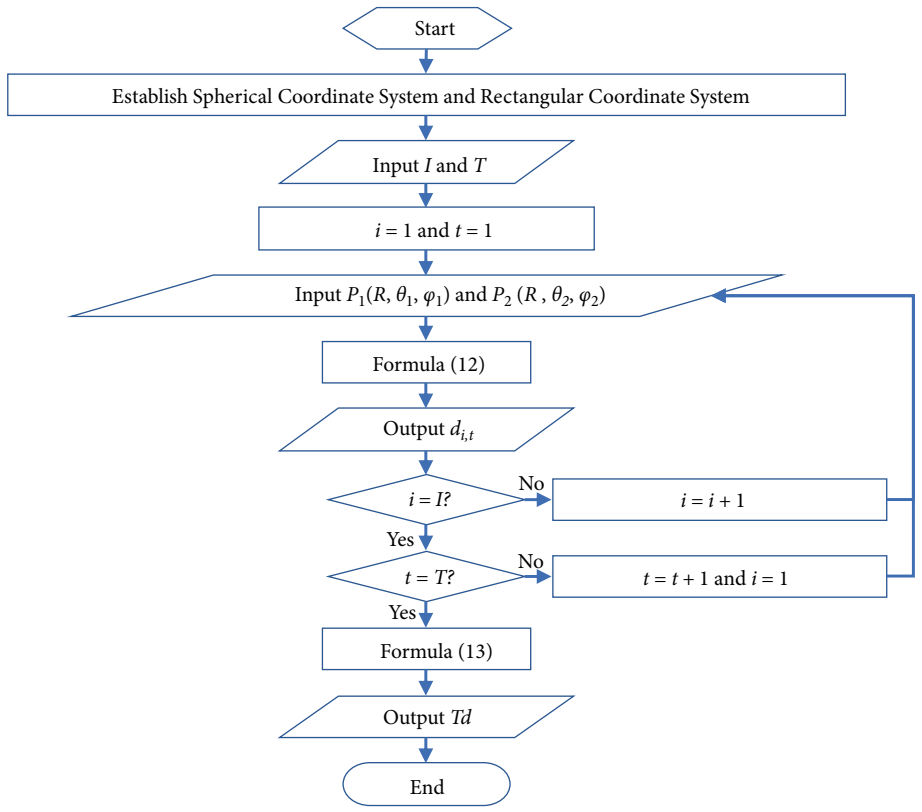

Figure 3: Flow chart of original model.

Fourth, considering the equation of arc length calculation, the distance between vectors $\overrightarrow{OP_1}$ and $\overrightarrow{OP_2}$ was calculated by Formula (11).

$$d = R\left\langle \overrightarrow{OP_1}, \overrightarrow{OP_2} \right\rangle. \tag{11}$$

Based on Formula (9), Formula (11) can be converted into Formula (12).

$$d = R \arccos\left(\sin\theta_1 \sin\theta_2 \cos\left(\varphi_2 - \varphi_1\right) + \cos\theta_1 \cos\theta_2\right). \tag{12}$$

In other words, the distance between $P_1(R, \theta_1, \varphi_1)$ and $P_2(R, \theta_2, \varphi_2)$ can be calculated approximately by the longitudes and latitudes of them based on GPS data, and the radius of the earth under Original Model.

Fifth, all the distances were summed up. Supposing that the variable Td represents total movements of vehicles under Original Model and it can be calculated by Formula (13).

$$Td = \sum_{i=1}^{I} \sum_{t=1}^{T} d_{i,t}. \tag{13}$$

3.4. Modified Digital Elevation Model. MDE adopts Original Model and SBI Model to improve the preciseness of results and it calculates distances in a comprehensive way (see Figure 4).

There are 5 steps in this section.

First, the Spherical Coordinate System was established in Formula (1).

Second, the Rectangular Coordinate System was established in Formula (4).

Third, all the unknown altitude values were calculated approximately by Spherical Bilinear Interpolation Model.

Fourth, the distance between P_1 and P_2 was calculated approximately by Modified Digital Elevation Model. Based on Formula (12), the distance between points $P_1(R + h_1, \theta_1, \varphi_1)$ and $P_2(R + h_2, \theta_2, \varphi_2)$ can be calculated by Formula (14) when $\rho = R + h_1$.

$$d|_{\rho = R + h_1} = (R + h_1) \arccos\left(\sin\theta_1 \sin\theta_2 \cos\left(\varphi_2 - \varphi_1\right) + \cos\theta_1 \cos\theta_2\right). \tag{14}$$

Based on Formula (12), the distance between points $P_1(R + h_1, \theta_1, \varphi_1)$ and $P_2(R + h_2, \theta_2, \varphi_2)$ can be calculated by Formula (15) when $\rho = R + h_2$.

$$d|_{\rho = R + h_2} = (R + h_2) \arccos\left(\sin\theta_1 \sin\theta_2 \cos\left(\varphi_2 - \varphi_1\right) + \cos\theta_1 \cos\theta_2\right). \tag{15}$$

Based on Distance Formula, the distance can be calculated by Formula (16).

$$d' = \sqrt{\left(\frac{d|_{\rho = R + h_1} + d|_{\rho = R + h_2}}{2}\right)^2 + (\Delta h)^2}. \tag{16}$$

Based on Formulas (14), (15), Formula (16) can be converted into Formula (17).

$$d' = \sqrt{\left[\left(R + \frac{h_1 + h_2}{2}\right) \arccos\left(\sin\theta_1 \sin\theta_2 \cos\left(\varphi_2 - \varphi_1\right) + \cos\theta_1 \cos\theta_2\right)\right]^2 + (h_2 - h_1)^2}. \tag{17}$$

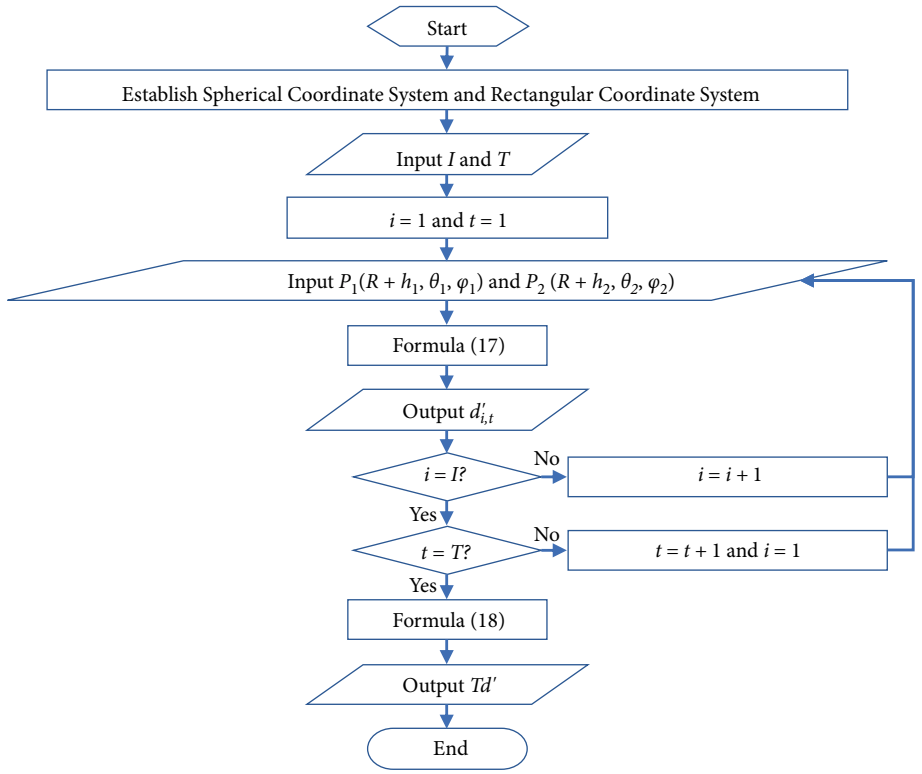

Figure 4: Flow chart of Modified Digital Elevation Model.

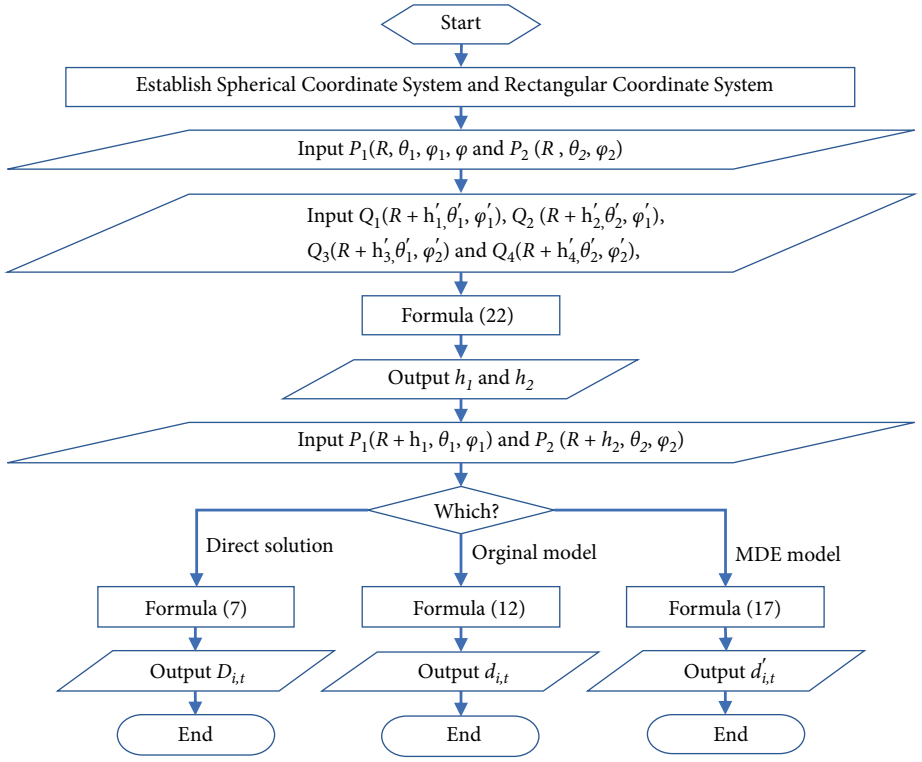

Figure 5: Flow chart of Spherical Bilinear Interpolation Model and its applications.

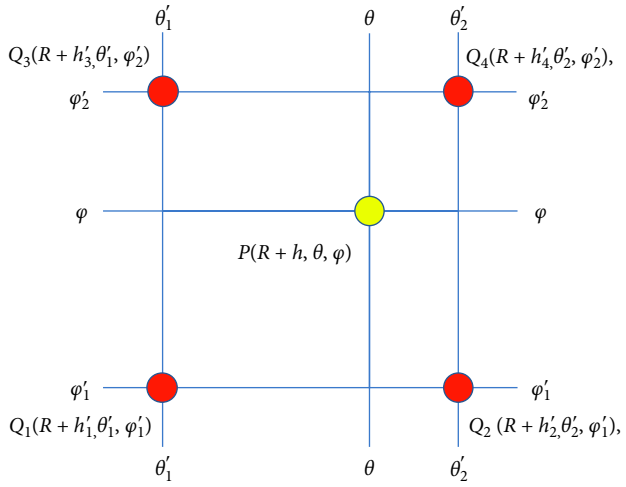

Figure 6: Schematic diagram of vertexes.

Fifth, all the distances were summed up. Supposing that the variable Td' represents total movements of vehicles under Modified Digital Elevation Model and it can be calculated by Formula (18).

$$Td' = \sum_{i=1}^{I} \sum_{t=1}^{T} d_{i,t}'. \tag{18}$$

3.5. Spherical Bilinear Interpolation Model. Spherical Bilinear Interpolation (SBI) Model helps improving the preciseness of GPS data with altitude especially when the data of altitudes is not precise enough or missing (see Figure 5).

There are 3 steps in this section.

First, find out 4 vertexes by positional notation based on the spherical coordinate of point P. For any point $P(R + h, \theta, \varphi)$ where $\theta_1' \le \theta \le \theta_2'$ and $\varphi_1' \le \varphi \le \varphi_2'$, there are 4 points $Q_1(R + h_1', \theta_1', \varphi_1')$, $Q_2(R + h_2', \theta_2', \varphi_1')$, $Q_3(R + h_3', \theta_1', \varphi_2')$, $Q_4(R + h_4', \theta_2', \varphi_2')$ around it (see Figure 6).

Second, figure out the relationship among the spherical coordinates of 5 points P, Q_1, Q_2, Q_3, Q_4. Supposing that there are 4 factors $\alpha_1, \alpha_2, \alpha_3, \alpha_4$ satisfying Formula (19).

$$\overrightarrow{OP} = \alpha_1 \overrightarrow{OQ_1} + \alpha_2 \overrightarrow{OQ_2} + \alpha_3 \overrightarrow{OQ_3} + \alpha_4 \overrightarrow{OQ_4}. \tag{19}$$

As a result, the solution of Formula (19) was settled by Formula (20). The derivation process of Formula (20) is in the Appendix (see Appendix B).

$$\begin{aligned}
\alpha_1 &= \frac{(\theta_2' - \theta) \times (\varphi_2' - \varphi)}{(\theta_2' - \theta_1') \times (\varphi_2' - \varphi_1')}, \\
\alpha_2 &= \frac{(\theta - \theta_1') \times (\varphi_2' - \varphi)}{(\theta_2' - \theta_1') \times (\varphi_2' - \varphi_1')}, \\
\alpha_3 &= \frac{(\theta_2' - \theta) \times (\varphi - \varphi_1')}{(\theta_2' - \theta_1') \times (\varphi_2' - \varphi_1')}, \\
\alpha_4 &= \frac{(\theta - \theta_1') \times (\varphi - \varphi_1')}{(\theta_2' - \theta_1') \times (\varphi_2' - \varphi_1')}.
\end{aligned} \tag{20}$$

Based on Formula (20), Formula (19) can be converted into Formula (21).

Figure 7: Actual position of the sample.

$$\begin{aligned}
\overrightarrow{OP} = {} & \frac{(\theta_2' - \theta) \times (\varphi_2' - \varphi)}{(\theta_2' - \theta_1') \times (\varphi_2' - \varphi_1')} \overrightarrow{OQ_1} \\
& + \frac{(\theta - \theta_1') \times (\varphi_2' - \varphi)}{(\theta_2' - \theta_1') \times (\varphi_2' - \varphi_1')} \overrightarrow{OQ_2} \\
& + \frac{(\theta_2' - \theta) \times (\varphi - \varphi_1')}{(\theta_2' - \theta_1') \times (\varphi_2' - \varphi_1')} \overrightarrow{OQ_3} \\
& + \frac{(\theta - \theta_1') \times (\varphi - \varphi_1')}{(\theta_2' - \theta_1') \times (\varphi_2' - \varphi_1')} \overrightarrow{OQ_4}.
\end{aligned} \tag{21}$$

The checking process of Formula (21) is in the Appendix (see Appendix C). Based on Formula (C.24) in the Appendix C, the altitude value of point $P(R + h, \theta, \varphi)$ can be calculated by Formula (22).

$$\begin{aligned}
h = {} & \frac{(\theta_2' - \theta) \times (\varphi_2' - \varphi)}{(\theta_2' - \theta_1') \times (\varphi_2' - \varphi_1')} \times h_1' + \frac{(\theta - \theta_1') \times (\varphi_2' - \varphi)}{(\theta_2' - \theta_1') \times (\varphi_2' - \varphi_1')} \\
& \times h_2' + \frac{(\theta_2' - \theta) \times (\varphi - \varphi_1')}{(\theta_2' - \theta_1') \times (\varphi_2' - \varphi_1')} \times h_3' + \frac{(\theta - \theta_1') \times (\varphi - \varphi_1')}{(\theta_2' - \theta_1') \times (\varphi_2' - \varphi_1')} \times h_4'.
\end{aligned} \tag{22}$$

Third, substitute h_1', h_2', h_3', h_4' by the altitude value of points Q_1, Q_2, Q_3, Q_4. Finally, the altitude value of point P can be calculated approximately by Spherical Bilinear Interpolation Model.

3.6. Data and Tools

(i) Data Source. The GPS data of taxis in this study was collected from the big data platform, Travel Cloud, which was developed by Ministry of Transport of the People's Republic of China (see Data Availability). It was provided in part by the transportation department of Liaoning Province, in part by Henan Province department of transportation, in part by Sanya Traffic and Transportation Bureau of Hainan Province. Its major data items include anonymous vehicle ID, longitude, latitude and recording time. And the digital elevation data in this study was collected from Google Map.

(ii) Data Processing. In terms of GPS data processing, there are 3 steps. First, all the taxi locations were averaged every 60 seconds so as to improve the accuracy of data, that is to say, average locations of those taxis were recorded every 60 seconds entirely. Second, the flaw data was removed so as to ensure the integrity of

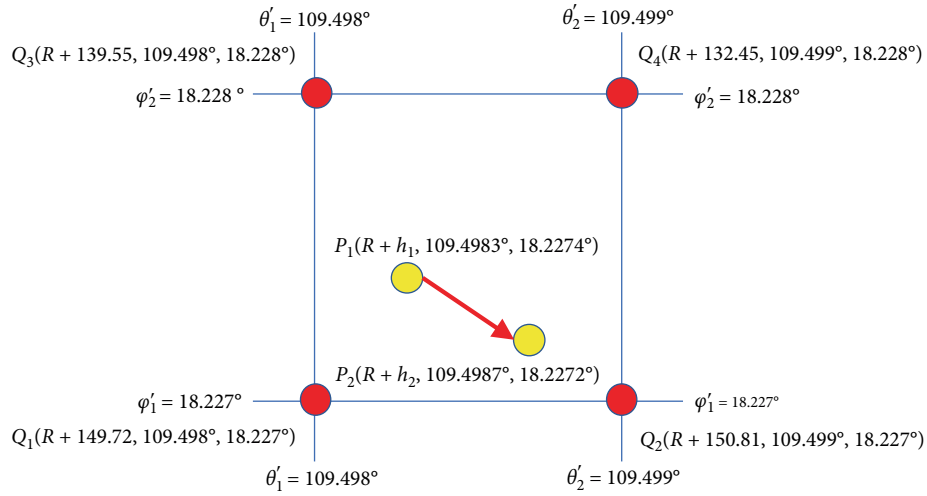

Figure 8: Schematic diagram of the sample.

data. Third, the obtained data was checked to avoid mistakes. As a result, GPS data without altitude was prepared. In terms of digital elevation data processing, there are 4 steps. First, the original digital elevation data was imported by Arcgis. Second, GPS data without altitude in a Microsoft Excel file was converted into a XY table of Arcgis geodatabase by the conversion tool called Excel to Table. Third, the XY table was adopted to create a point feature class on the basis of its coordinate system, World Geodetic System 1984 by the data management tool called Add XY Data. Fourth, the altitude data of the point feature class was extracted by the spatial analyst tool called Extract Values by Points. As a result, GPS data with altitude was prepared (see the file named "Data.xlsx" in the Supplementary Material).

(iii) Implement Tool. Several kinds of software were adopted in this study as follows. Rivermap X3.1 was applied for extracting the altitude from digital elevation data. Microsoft Excel 2019 was applied for original data processing and result storage. Stata 14.1 was applied for statistic analyzing. Matlab R2018a was applied for programming. Global Mapper 14.1 was applied for map drawing. Arcgis Pro 2.2.0 (trial version) was applied for map drawing and spatial analyzing.

4. Results

In this section, a sample (see Section 4.1) was presented for better description and vehicle movements were analyzed by Direct Solution, Original Model, MDE model at the same time, including Sanya (see Section 4.2), Zhengzhou (see Section 4.3), Liaoyang (see Section 4.4). And the results of them were compared with each other (see Section 4.5).

4.1. Sample. In the sample, there was a taxi around Luhuitou Park in Sanya of Hainan Province moving from the left yellow point to the right yellow point (see Figure 7). Luhuitou Park was on a hill and the taxi was on the road uphill. It indicated that the altitude of the taxi in the sample would rise from the left yellow point to the right yellow point.

In Figure 7, Luhuitou Park was surrounded by South of Sea Road, also known as Nanbianhai Road in Chinese. Furthermore, four red points surrounding yellow points were supplementary points drawn for SBI Model. Their longitudes and latitudes kept only 3 decimal digits. Actual position in Figure 3 can be converted into Schematic diagram (see Figure 8).

In Figure 8, there are 2 yellow points $P_1(R + h_1, 109.4983^{\circ}, 18.2274^{\circ})$, $P_2(R + h_2, 109.4987^{\circ}, 18.2272^{\circ})$ and 4 red points $Q_1(R + 152, 109.498^{\circ}, 18.227^{\circ})$, $Q_2(R + 150.81, 109.499^{\circ}, 18.227^{\circ})$, $Q_3(R + 139.55, 109.498^{\circ}, 18.228^{\circ})$, $Q_4(R + 132.45, 109.499^{\circ}, 18.228^{\circ})$.

According to the original digital elevation data, the altitude value of points P_1 and P_2 were 145 (m) and 147 (m) respectively. The taxi altitude in the sample changed approximately 2 (m) from P_1 to P_2. Based on SBI Model, the altitude value of points P_1 and P_2 can be further calculated by Formula (17). And the altitude value of points P_1 and P_2 adjusted by SBI Model were 145.00 (m) and 147.30 (m) respectively. Based on Formulas (7), (12), (17), the sample results and comparisons of three methods were figured out (see Table 2). The derivation process of Table 2 is in the Appendix (see Appendix D).

In Table 2, Value1 adopted original digital elevation data while Value2 adopted the digital elevation data adjusted by SBI Model. Under Value1, the vehicle movement $\overrightarrow{P_1P_2}$ under Direct Solution was 49.267562 (m). The deviation between Original Model and Direct Solution was 0.041677 (m) while the deviation between MDE Model and Direct Solution was only 0.000061 (m). Under Value2, the vehicle movement $\overrightarrow{P_1P_2}$ under Direct Solution was 49.280653 (m). The deviation between Original Model and Direct Solution was 0.054768 (m) while the deviation between MDE Model and Direct Solution was only 0.000062 (m). It can be seen that MDE Model had much less disparity with Direct Solution than Original Model in the sample results. In addition, even if the original digital elevation data, the altitude value of points P_1 and P_2 was

Table 2: Sample results and comparisons of three methods. Unit: m.

Method	Variable	Value1	Value2	|Value1 − Value2|
Direct Solution	D	49.267562	49.280653	0.013091
Original Model	d	49.225885	49.225885	0
MDE Model	d'	49.267623	49.280715	0.013092
(Comparisons)	$\|D - d\|$	0.041677	0.054768	0.013091
	$\|D - d'\|$	0.000061	0.000062	0.000001

Table 3: Sanya results and comparisons of three methods. Unit: m.

Method	Variable	Value1	Value2	|Value1 − Value2|
Direct Solution	TD	34,065,354.87	34,064,690.71	664.16
Original Model	Td	34,058,703.99	34,058,703.99	0
MDE Model	Td'	34,065,343.29	34,064,679.28	664.01
(Comparisons)	$\|TD - Td\|$	6,650.88	5,986.72	664.16
	$\|TD - Td'\|$	11.58	11.43	0.15

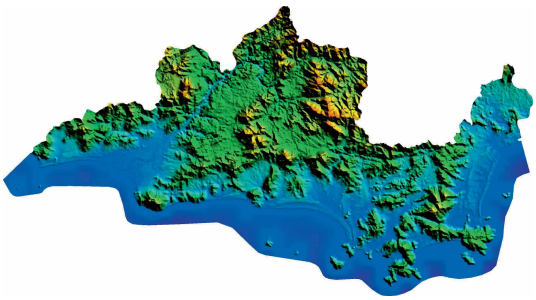

Figure 9: Elevation map of Sanya.

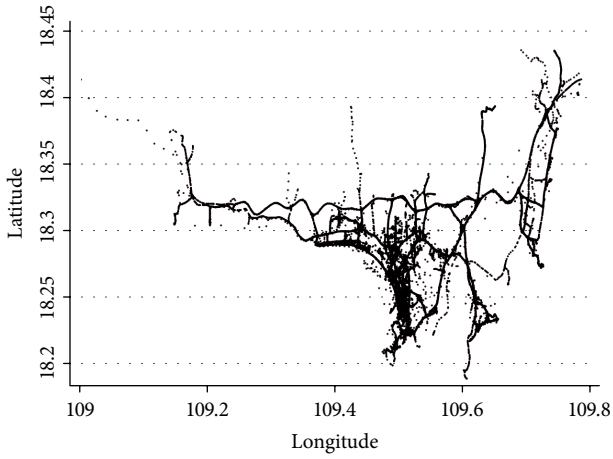

Figure 10: Taxi positions of Sanya.

missing, it could be further calculated by SBI Model. By contrast, the deviation between Original Model and Direct Solution was 0.013091 (m) while the deviation between MDE Model and Direct Solution was only 0.000001 (m). It further verified the advantage of MDE Model even though some data was missing in the sample results and SBI Model was adopted to improve the preciseness of GPS data with altitude.

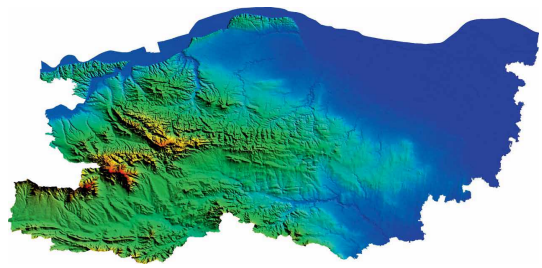

Figure 11: Elevation map of Zhengzhou.

The deviation between Original Model and MDE Model may be more obvious when sample size increases.

4.2. Sanya. Sanya is a city in Hainan Province where the longitude was in the range of [108.928°, 109.807°] while the latitude was in the range of [18.144°, 18.625°]. It located in the southern China and its altitudes had differences. (see Figure 9).

In Figure 9, colors reflected the elevation. The altitudes of blue area were low. The altitudes of green area were medium. The altitudes of yellow area were high.

In the origin data of Sanya, the locations of 2,506 taxis were recorded every 15 seconds from 9:00 a.m. to 9:59 a.m. on Nov. 15th in 2016, adding up to 766,042 records (see Figure 10).

In Figure 10, taxi positions of Sanya located minutely at a fixed monitor where the longitude was in the range of [109.0°, 109.8°] while the latitude was in the range of [18.1°, 18.5°]. After data processing, there were 2,191 taxis and 131,460 records left in the experimental data. And 107,427 movements of 2,096 taxis were extracted as a result. Based on Formulas (7), (12), (17), the Sanya results and comparisons of three methods were figured out (see Table 3).

In Table 3, Value1 adopted original digital elevation data while Value2 adopted the digital elevation data adjusted by SBI Model. Under Value1, total vehicle movements under Direct Solution was 34, 065, 354.87 (m). The deviation between Original Model and Direct Solution was 6, 650.88 (m) while the deviation between MDE Model and Direct Solution was only

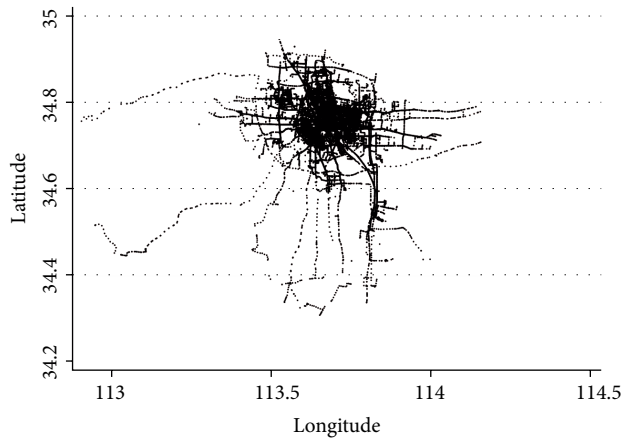

Figure 12: Taxi positions of Zhengzhou.

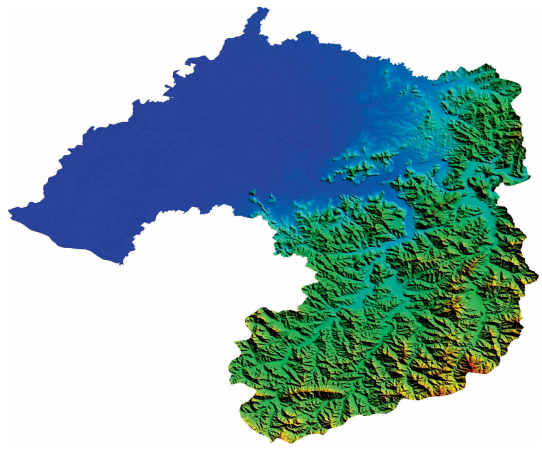

Figure 13: Elevation map of Liaoyang.

Table 4: Zhengzhou results and comparisons of three methods. Unit: m.

Method	Variable	Value1	Value2	|Value1 − Value2|
Direct Solution	TD	94,767,484.51	94,767,008.47	476.04
Original Model	Td	94,764,096.35	94,764,096.35	0
MDE Model	Td'	94,767,481.20	94,767,005.17	476.03
(Comparisons)	$\|TD - Td\|$	3,388.16	2,912.12	476.04
	$\|TD - Td'\|$	3.31	3.30	0.01

11.58 (m). Under Value2, total vehicle movements under Direct Solution was 34, 064, 690.71 (m). The deviation between Original Model and Direct Solution was 5, 986.72 (m) while the deviation between MDE Model and Direct Solution was only 11.43 (m). It can be seen that the deviation between Original Model and MDE Model in Sanya was much more obvious than sample. The results in Sanya verified that MDE Model had much less disparity with Direct Solution than Original Model. In addition, even if some original digital elevation data of actual positions in Sanya were missing, it could be further calculated by SBI Model. By contrast, the deviation between Original Model and Direct Solution was 664.16 (m) while the deviation between MDE Model and Direct Solution was only 0.15 (m). It further verified the advantage of MDE Model even though some data was missing in Sanya and SBI Model was adopted to improve the preciseness of GPS data with altitude.

4.3. Zhengzhou. Zhengzhou is a city in Henan Province where the longitude was in the range of [112.714°, 114.206°] while the latitude was in the range of [34.262°, 34.985°]. It located in the midland China and its altitudes had differences. (see Figure 11).

In Figure 11, colors reflected the elevation. The altitudes of blue area were low. The altitudes of green area were medium. The altitudes of yellow area were high.

In the origin data of Zhengzhou, the locations of 9,703 taxis were recorded every 15 seconds from 14:50 p.m. to 15:38 p.m. on Nov. 15th in 2016, adding up to 1,048,575 records (see Figure 12).

In Figure 12, taxi positions of Zhengzhou located minutely at a fixed monitor where the longitude was in the range of [112.8°, 114.5°] while the latitude was in the range of [34.2°, 35.0°]. After data processing, there were 5,774 taxis and 282,926 records left in the experimental data. And 229,370 movements of 5,597 taxis were extracted as a result. Based on Formulas (7), (12), (17), the Zhengzhou results and comparisons of three methods were figured out (see Table 4).

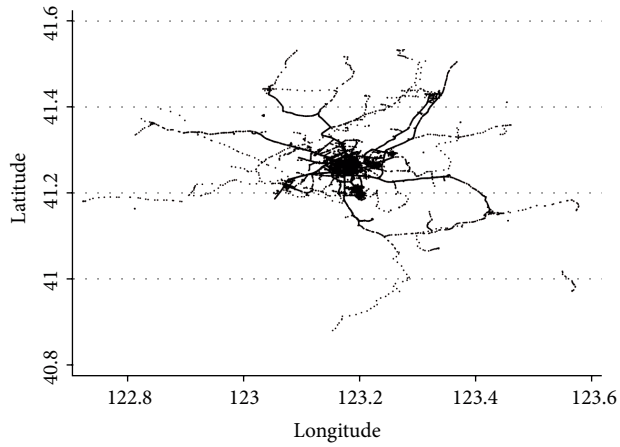

Figure 14: Taxi positions of Liaoyang.

In Table 4, Value1 adopted original digital elevation data while Value2 adopted the digital elevation data adjusted by SBI Model. Under Value1, total vehicle movements under Direct Solution was 94,767,484.51 (m). The deviation between Original Model and Direct Solution was 3,388.16 (m) while the deviation between MDE Model and Direct

Table 5: Liaoyang results and comparisons of three methods. Unit: m.

Method	Variable	Value1	Value2	|Value1 − Value2|
Direct Solution	TD	29,796,201.87	29,796,059.67	142.20
Original Model	Td	29,795,356.19	29,795,356.19	0
MDE Model	Td'	29,796,201.11	29,796,058.91	142.20
(Comparisons)	$\|TD - Td\|$	845.68	703.48	142.20
	$\|TD - Td'\|$	0.76	0.76	0.00

Table 6: Comprehensive results and comparisons of three methods. Unit: m.

Variable	Data	Sanya	Zhengzhou	Liaoyang	Total
$\|TD - Td\|$	Value1	6,650.88	3,388.16	845.68	10,884.72
	Value2	5,986.72	2,912.12	703.48	9,602.32
$\|TD - Td'\|$	Value1	11.58	3.31	0.76	15.65
	Value2	11.43	3.30	0.76	15.49
$\frac{\|TD-Td'\|}{\|TD-Td\|}$	Value1	0.17%	0.10%	0.09%	0.14%
	Value2	0.19%	0.11%	0.11%	0.16%

Solution was only 3.31 (m). Under Value2, total vehicle movements under Direct Solution was 94,767,008.47 (m). The deviation between Original Model and Direct Solution was 2,912.12 (m) while the deviation between MDE Model and Direct Solution was only 3.30 (m). It can be seen that the deviation between Original Model and MDE Model in Zhengzhou was much more obvious than sample. The results in Zhengzhou verified that MDE Model had much less disparity with Direct Solution than Original Model. In addition, even if some original digital elevation data of actual positions in Zhengzhou were missing, it could be further calculated by SBI Model. By contrast, the deviation between Original Model and Direct Solution was 476.04 (m) while the deviation between MDE Model and Direct Solution was only 0.01 (m). It further verified the advantage of MDE Model even though some data was missing in Zhengzhou and SBI Model was adopted to improve the preciseness of GPS data with altitude.

4.4. Liaoyang. Liaoyang is a city in Liaoning Province where the longitude was in the range of [112.588°, 123.684°] while the latitude was in the range of [40.710°, 41.615°]. It located in the northern China and its altitudes had differences. (see Figure 13).

In Figure 13, colors reflected the elevation. The altitudes of blue area were low. The altitudes of green area were medium. The altitudes of yellow area were high.

In the origin data of Liaoyang, the locations of 2,237 taxis were recorded every 30 seconds from 9:59 a.m. to 10:58 a.m. on Aug. 8th in 2016, adding up to 268,440 records (see Figure 14).

In Figure 14, taxi positions of Liaoyang located minutely at a fixed monitor where the longitude was in the range of [122.7°, 123.6°] while the latitude was in the range of [40.8°, 41.6°]. After data processing, there were 2,025 taxis and 121,440 records left in the experimental data. And 87,879 movements of 1,810 taxis were extracted as a result. Based on Formulas (7), (12), (17), the Liaoyang results and comparisons of three methods were figured out (see Table 5).

In Table 5, Value1 adopted original digital elevation data while Value2 adopted the digital elevation data adjusted by SBI Model. Under Value1, total vehicle movements under Direct Solution was 29,796,201.87 (m). The deviation between Original Model and Direct Solution was 845.68 (m) while the deviation between MDE Model and Direct Solution was only 0.76 (m). Under Value2, total vehicle movements under Direct Solution was 29,796,059.67 (m). The deviation between Original Model and Direct Solution was 703.48 (m) while the deviation between MDE Model and Direct Solution was only 0.76 (m). It can be seen that the deviation between Original Model and MDE Model in Liaoyang was much more obvious than sample. The results in Liaoyang verified that MDE Model had much less

Table 7: Notations for variables.

Notation	Explanation
O	The center of coordinate systems/the center of the earth
P	The location
ρ	The radial distance
θ	The polar angle
φ	The azimuthal angle
R	The radius of the earth
h	The altitude
P_i	The location of vehicles
Q_i	The location near the location of vehicles
θ_i	The longitude of the location of vehicles
φ_i	The latitude of the location of vehicles
h_i	The altitude of the location of vehicles
i	The vehicle ID number
t	The time
I	The maximum of vehicle ID number
T	The maximum of time
D	Movements between two locations of vehicles under Direct Solution
d	Movements between two locations of vehicles under Original Model
d'	Movements between two locations of vehicles under Modified Digital Elevation Model
TD	Total movements under Direct Solution
Td	Total movements under Original Model
Td'	Total movements under Modified Digital Elevation Model

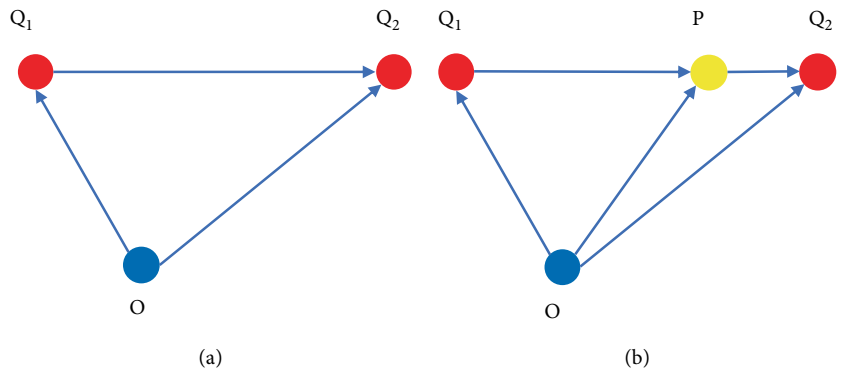

FIGURE 15: Schematic diagram for the derivation process of Formula (B.6). (a) Original condition. (b) Add the point P on the line Q_1Q_2.

disparity with Direct Solution than Original Model. In addition, even if some original digital elevation data of actual positions in Liaoyang were missing, it could be further calculated by SBI Model. By contrast, the deviation between Original Model and Direct Solution was 142.20 (m) while the deviation between MDE Model and Direct Solution was less than 0.01 (m). It further verified the advantage of MDE Model even though some data was missing in Liaoyang and SBI Model was adopted to improve the preciseness of GPS data with altitude.

4.5. Comparisons. Based on Tables 3–5, the Comprehensive results and comparisons of three methods were figured out (see Table 6).

In Table 6, Value1 adopted original digital elevation data while Value2 adopted the digital elevation data adjusted by SBI Model. Under Value1, total deviation between Original Model and Direct Solution was 10,884.72 (m) while total deviation between MDE Model and Direct Solution was only 15.65 (m). The latter is 0.14% that of the former. Under Value2, total deviation between Original Model and Direct Solution was 9,602.32 (m) while total deviation between MDE Model and Direct Solution was only 15.49 (m). The latter is 0.16% that of the former. Comprehensive results verified that MDE Model had over 99% less disparity with Direct Solution than Original Model because MDE Model took altitude into consideration but Original Model did not. In other words, MDE Model was much more accurate than Original Model.

5. Discussion

In this section, several operational details over the course of this research were presented for fellow colleagues and follow-up studies (see Section 5.1). In addition, the authors discussed the application prospects in the field of automatic vehicles (see Section 5.2).

5.1. Operational Details. Over the course of this research, there were several operational details that had not been contemplated within, including software use and data processing, which are described as follows.

(i) During processing original data by Microsoft Excel 2019, we found that Excel had a processing limit that its maximum capacity was 1,048,576 rows. If original data exceeds this limit, we had to divide them into several pieces before processing. Otherwise, there were other software, Snapde for instance, suiting for the big data more than 1,048,576 rows. In this research, the biggest original data was 1,048,575 records in Zhengzhou (see Section 4.3). Therefore, we adopted Excel as a result.

(ii) During spatial analyzing by Arcgis Pro (trial version), we found that the function of the spatial analyst tool called Extract Values by Points was available in v2.2.0 but unavailable in v2.3.0. Some errors may exist in v2.3.0. Therefore, we adopted v2.2.0 as a result.

(iii) In SBI Model, the first step was to find out 4 vertexes by positional notation based on the spherical coordinate of point P. We tried both 3 decimal digits and 4 decimal digits and found that 3 decimal digits of longitudes and latitudes were sufficient for vertexes.

(iv) In this research, we defined that $R = 6378137.00$ (m), which represents the radius of the earth (see Section 3.2). However, the radius of the earth has differences in different places.

5.2. Application Prospects. In the field of automatic vehicles, vehicle security is always under the spotlight. And elevation changes have a significant effect on the security of automatic vehicles because it is difficult for them to respond as human beings when traffic changes. Most crucially, the specific calculations used to vehicle movement analyses must be not only accurate but also fast. Otherwise, those automatic vehicles will be in danger, especially when they are running at high speed. Thus, appropriate counter measures could be taken to suppress or reverse or at least alleviate its limitations. The application prospects had not been contemplated within former sections, including MDE Model and SBI Model, which are described as follows.

(i) MDE Model. In last section, results verified that altitude was a key element of vehicle movement analyses, and it indicated that MDE Model was much more accurate than Original Model in terms of vehicle movement analysis (see Section 4.2–4.5). It is technically feasible to send alerts to the automatic vehicles

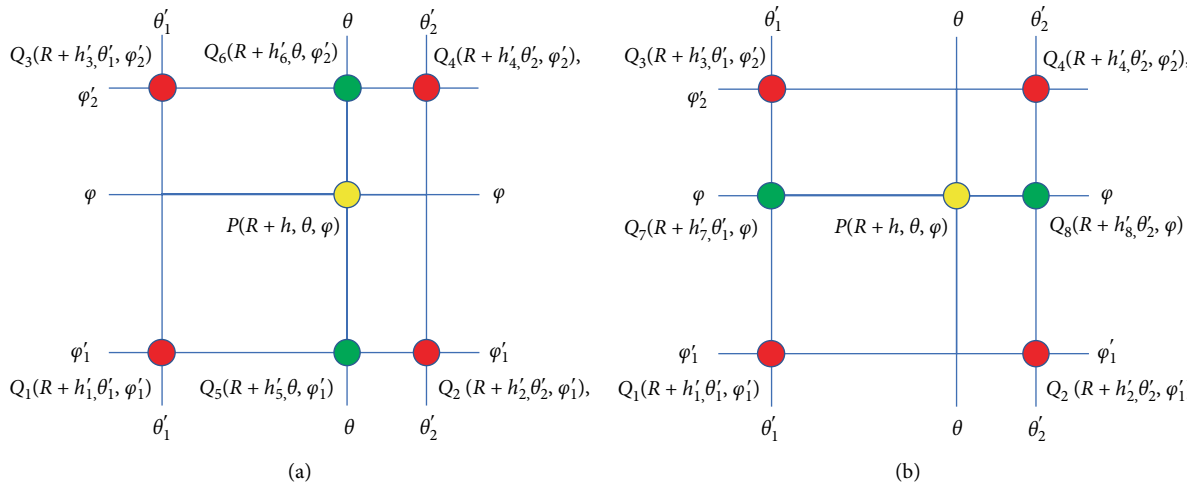

FIGURE 16: Schematic diagram for the derivation process of Formula (19). (a) Add two green points Q_5 and Q_6 where their polar angles are equivalent to θ. (b) Add two green points Q_7 and Q_8 where their azimuthal angles are equivalent to φ.

on the road uphill or downhill in advance so that they can adjust their brake systems in time. Compared with Direct Solution, MDE Model reduced the computational costs by avoiding square algorithms. Compared with Original Model, MDE Model raised the computational accuracy by taking altitude into consideration. Thus, analyzing vehicle movements by MDE Model could be faster and more accurate and it has a bright future in the field of automatic vehicles.

(ii) SBI Model. In last section, results indicated that SBI Model could improve the preciseness of GPS data with altitude especially when some data was missing in terms of vehicle movement Analysis (see Section 4.2–4.4). It is technically feasible for automatic vehicles to establish an offline GIS database and evaluate real-time GIS information when complete data is difficult to acquire, in the boondocks for instance, so that they can make vehicle movement analyses continuously. SBI Model can be viewed as a supplementary for MDE Model. Thus, SBI Model is necessary in the field of vehicle movement analyses and it also has a bright future in the field of automatic vehicles.

To sum up, the authors discussed that MDE Model and SBI Model have great practical prospects and they are suitable and useful for autonomous vehicles, especially for automatic taxis.

6. Conclusions

In this study, the authors proposed Modified Digital Elevation (MDE) Model, Spherical Bilinear Interpolation (SBI) Model and adopted the experimental data of 9,990 GPS-enabled taxis in Sanya, Zhengzhou and Liaoyang to make movement comparisons by three methods, including Direct Solution, Original Model and MDE Model. MDE Model was for improving the accuracy of vehicle movement analyses. SBI Model was for further improving the preciseness of GPS data with altitude. Given the arguments above mentioned, the major findings in this article include several contents, which are described as follows.

(i) The application of MDE Model could improve the accuracy of vehicle movement analyses and it resulted in over 99% less disparity with Direct Solution than Original Model because it took altitude into consideration (see Section 4.2–4.5).

(ii) The application of SBI Model could improve the preciseness of GPS data with altitude especially when some data was missing (see Section 4.2–4.4).

(iii) The application of MDE Model and SBI Model could improve effects according to statistic results (see Section 5.2) and it has a bright future in the field of automatic vehicles.

The contributions of this study could be as follows:

(i) MDE Model was built to calculate vehicle movements by digital elevation data based on mathematical equations (see Section 3.4).

(ii) SBI Model was proposed and applied to improve the preciseness of GPS data with altitude of collaborative vehicles (see Section 3.5).

(iii) A sample was presented for better description (see Section 4.1).

(iv) It was verified that MDE Model had higher accuracy than the original (see Section 4.2–4.5).

(v) The Derivation Process and Checking Process of SBI Model was proposed (see Appendix C, D).

Future directions for research can be in two ways. The one is improving MDE Model and SBI Model. The other is expanding the data size.

Appendix

A. Notations for Variables

In Appendix A, notations for variables are presented (see Table 7).

B. Derivation Process of Formula (20)

In Appendix B, a series of formulas are built to find out the solution of Formula (19) and work out Formula (20).

Supposing that the point O is the center of the coordinate system and there are two points Q_1 and Q_2 (see Figure 15(a)). Supposing that the point P is on the line Q_1Q_2, and points Q_1, P and Q_2 are collinear (see Figure 15(b)).

Based on Vector Addition Formula, the relations between $\overrightarrow{OQ_1}$, $\overrightarrow{OQ_2}$, and $\overrightarrow{Q_1Q_2}$ can be expressed by Formula (B.1). In the same way, the relations between $\overrightarrow{OP}$, $\overrightarrow{OQ_1}$, and $\overrightarrow{Q_1P}$ can be expressed by Formula (B.2).

$$\overrightarrow{OQ_1} + \overrightarrow{Q_1Q_2} = \overrightarrow{OQ_2}, \tag{B.1}$$

$$\overrightarrow{OP} = \overrightarrow{OQ_1} + \overrightarrow{Q_1P}. \tag{B.2}$$

Supposing that λ is the proportion of P in the vector $\overrightarrow{Q_1Q_2}$ as Formula (B.3).

$$\lambda = \frac{|Q_1P|}{|Q_1Q_2|}. \tag{B.3}$$

Based on Vector Proportion Formula, the relations between $\overrightarrow{Q_1P}$ and $\overrightarrow{Q_1Q_2}$ can be expressed by Formula (B.4).

$$\overrightarrow{Q_1P} = \lambda\overrightarrow{Q_1Q_2}, \tag{B.4}$$

where $0 \le \lambda \le 1$. Based on Formulas (B.2, B.4), $\overrightarrow{OP}$ can be calculated by Formula (B.5).

$$\overrightarrow{OP} = \overrightarrow{OQ_1} + \lambda\left(\overrightarrow{OQ_2} - \overrightarrow{OQ_1}\right). \tag{B.5}$$

Formula (B.5) can be simplified into Formula (B.6).

$$\overrightarrow{OP} = (1-\lambda)\overrightarrow{OQ_1} + \lambda\overrightarrow{OQ_2}. \tag{B.6}$$

In order to find out the solution of Formula (18) based on Formula (B.6), there are two plans for the derivation process of Formula (19), called Plan A and Plan B.

Plan A adds two green points $Q_5(R + h_5', \theta, \varphi_1')$ and $Q_6(R + h_6', \theta, \varphi_2')$ on the basis of Figure 1 where their azimuthal angles are equivalent to φ (see Figure 16(a)). In this way, points Q_1, Q_5, Q_2 are collinear, points Q_3, Q_6, Q_4 are collinear, besides, points Q_5, P, Q_6 are collinear. Based on Formula (B.6), $\overrightarrow{OQ_5}$, $\overrightarrow{OQ_6}$, and $\overrightarrow{OP}$ can be calculated respectively by Formulas (B.7), (B.8), (B.9).

$$\overrightarrow{OQ_5} = \frac{|Q_5Q_2|}{|Q_1Q_2|}\overrightarrow{OQ_1} + \frac{|Q_1Q_5|}{|Q_1Q_2|}\overrightarrow{OQ_2}, \tag{B.7}$$

$$\overrightarrow{OQ_6} = \frac{|Q_6Q_4|}{|Q_3Q_4|}\overrightarrow{OQ_3} + \frac{|Q_3Q_6|}{|Q_3Q_4|}\overrightarrow{OQ_4}, \tag{B.8}$$

$$\overrightarrow{OP} = \frac{|PQ_6|}{|Q_5Q_6|}\overrightarrow{OQ_5} + \frac{|Q_5P|}{|Q_5Q_6|}\overrightarrow{OQ_6}. \tag{B.9}$$

Based on Formulas (B.7), (B.8), Formula (B.9) can be converted into Formula (B.10).

$$\overrightarrow{OP} = \frac{|PQ_6|}{|Q_5Q_6|} \times \left(\frac{|Q_5Q_2|}{|Q_1Q_2|}\overrightarrow{OQ_1} + \frac{|Q_1Q_5|}{|Q_1Q_2|}\overrightarrow{OQ_2}\right) + \frac{|Q_5P|}{|Q_5Q_6|} \times \left(\frac{|Q_6Q_4|}{|Q_3Q_4|}\overrightarrow{OQ_3} + \frac{|Q_3Q_6|}{|Q_3Q_4|}\overrightarrow{OQ_4}\right). \tag{B.10}$$

Formula (B.10) can be converted into Formula (B.11).

$$\overrightarrow{OP} = \frac{|PQ_6| \times |Q_5Q_2|}{|Q_5Q_6| \times |Q_1Q_2|}\overrightarrow{OQ_1} + \frac{|PQ_6| \times |Q_1Q_5|}{|Q_5Q_6| \times |Q_1Q_2|}\overrightarrow{OQ_2} + \frac{|Q_5P| \times |Q_6Q_4|}{|Q_5Q_6| \times |Q_3Q_4|}\overrightarrow{OQ_3} + \frac{|Q_5P| \times |Q_3Q_6|}{|Q_5Q_6| \times |Q_3Q_4|}\overrightarrow{OQ_4}. \tag{B.11}$$

Considering $|Q_1Q_2| = |Q_3Q_4| = \theta_2' - \theta_1'$, $|Q_1Q_5| = |Q_3Q_6| = \theta - \theta_1'$ $|Q_5Q_2| = |Q_6Q_4| = \theta_2' - \theta$, $|Q_5P| = \varphi - \varphi_1'$, and $|PQ_6| = \varphi_2' - \varphi$, Formula (B.11) can be converted into Formula (B.12).

$$\overrightarrow{OP} = \frac{(\varphi_2' - \varphi) \times (\theta_2' - \theta)}{(\varphi_2' - \varphi_1') \times (\theta_2' - \theta_1')}\overrightarrow{OQ_1} + \frac{(\varphi_2' - \varphi) \times (\theta - \theta_1')}{(\varphi_2' - \varphi_1') \times (\theta_2' - \theta_1')}\overrightarrow{OQ_2} + \frac{(\varphi - \varphi_1') \times (\theta_2' - \theta)}{(\varphi_2' - \varphi_1') \times (\theta_2' - \theta_1')}\overrightarrow{OQ_3} + \frac{(\varphi - \varphi_1') \times (\theta - \theta_1')}{(\varphi_2' - \varphi_1') \times (\theta_2' - \theta_1')}\overrightarrow{OQ_4}. \tag{B.12}$$

Plan B adds two green points $Q_7(R + h_7', \theta_1', \varphi)$ and $Q_8(R + h_8', \theta_2', \varphi)$ on the basis of Figure 1 where their azimuthal angles are equivalent to φ (see Figure 16(b)). In this way, points Q_1, Q_7, Q_3 are collinear, points Q_2, Q_8, Q_4 are collinear, besides, points Q_7, P, Q_8 are collinear. Based on Formula (B.6), $\overrightarrow{OQ_7}$, $\overrightarrow{OQ_8}$, and $\overrightarrow{OP}$ can be calculated respectively by Formulas (B.13), (B.14), (B.15).

$$\overrightarrow{OQ_7} = \frac{|Q_7Q_3|}{|Q_1Q_3|}\overrightarrow{OQ_1} + \frac{|Q_1Q_7|}{|Q_1Q_3|}\overrightarrow{OQ_3}, \tag{B.13}$$

$$\overrightarrow{OQ_8} = \frac{|Q_8Q_4|}{|Q_2Q_4|}\overrightarrow{OQ_2} + \frac{|Q_2Q_8|}{|Q_2Q_4|}\overrightarrow{OQ_4}, \tag{B.14}$$

$$\overrightarrow{OP} = \frac{|PQ_8|}{|Q_7Q_8|}\overrightarrow{OQ_7} + \frac{|Q_7P|}{|Q_7Q_8|}\overrightarrow{OQ_8}. \tag{B.15}$$

Based on Formulas (B.13), (B.14), Formula (B.15) can be converted into Formula (B.16).

$$\overrightarrow{OP} = \frac{|PQ_8|}{|Q_7Q_8|} \times \left(\frac{|Q_7Q_3|}{|Q_1Q_3|}\overrightarrow{OQ_1} + \frac{|Q_1Q_7|}{|Q_1Q_3|}\overrightarrow{OQ_3}\right) + \frac{|Q_7P|}{|Q_7Q_8|} \times \left(\frac{|Q_8Q_4|}{|Q_2Q_4|}\overrightarrow{OQ_2} + \frac{|Q_2Q_8|}{|Q_2Q_4|}\overrightarrow{OQ_4}\right). \tag{B.16}$$

Formula (B.16) can be converted into Formula (B.17).

$$\overrightarrow{OP} = \frac{|PQ_8| \times |Q_7Q_3|}{|Q_7Q_8| \times |Q_1Q_3|} \overrightarrow{OQ_1} + \frac{|Q_7P| \times |Q_8Q_4|}{|Q_7Q_8| \times |Q_2Q_4|} \overrightarrow{OQ_2} + \frac{|PQ_8| \times |Q_1Q_7|}{|Q_7Q_8| \times |Q_1Q_3|} \overrightarrow{OQ_3} + \frac{|Q_7P| \times |Q_2Q_8|}{|Q_7Q_8| \times |Q_2Q_4|} \overrightarrow{OQ_4}. \tag{B.17}$$

Considering $|Q_1Q_3| = |Q_2Q_4| = \varphi_2' - \varphi_1'$, $|Q_1Q_7| = |Q_2Q_8| = \varphi - \varphi_1'$ $|Q_7Q_3| = |Q_8Q_4| = \varphi_2' - \varphi$, $|Q_7P| = \theta - \theta_1'$, and $|PQ_8| = \theta_2' - \theta$, Formula (B.17) can be converted into Formula (B.18).

$$\overrightarrow{OP} = \frac{(\theta_2' - \theta) \times (\varphi_2' - \varphi)}{(\theta_2' - \theta_1') \times (\varphi_2' - \varphi_1')} \overrightarrow{OQ_1} + \frac{(\theta - \theta_1') \times (\varphi_2' - \varphi)}{(\theta_2' - \theta_1') \times (\varphi_2' - \varphi_1')} \overrightarrow{OQ_2} + \frac{(\theta_2' - \theta) \times (\varphi - \varphi_1')}{(\theta_2' - \theta_1') \times (\varphi_2' - \varphi_1')} \overrightarrow{OQ_3} + \frac{(\theta - \theta_1') \times (\varphi - \varphi_1')}{(\theta_2' - \theta_1') \times (\varphi_2' - \varphi_1')} \overrightarrow{OQ_4}. \tag{B.18}$$

Compare Formula (B.12) with Formula (B.18), it can be concluded that plan A and plan B have the same result. And then α_1, α_2, α_3, and α_4 can be calculated respectively by Formulas (B.19), (B.20), (B.21), (B.22).

$$\alpha_1 = \frac{(\theta_2' - \theta) \times (\varphi_2' - \varphi)}{(\theta_2' - \theta_1') \times (\varphi_2' - \varphi_1')}, \tag{B.19}$$

$$\alpha_2 = \frac{(\theta - \theta_1') \times (\varphi_2' - \varphi)}{(\theta_2' - \theta_1') \times (\varphi_2' - \varphi_1')}, \tag{B.20}$$

$$\alpha_3 = \frac{(\theta_2' - \theta) \times (\varphi - \varphi_1')}{(\theta_2' - \theta_1') \times (\varphi_2' - \varphi_1')}, \tag{B.21}$$

$$\alpha_4 = \frac{(\theta - \theta_1') \times (\varphi - \varphi_1')}{(\theta_2' - \theta_1') \times (\varphi_2' - \varphi_1')}. \tag{B.22}$$

As a result, the solution of Formula (19) was settled by Formula (20) on the basis of Formulas (B.19), (B.20), (B.21), (B.22).

C. Checking Process of Formula (21)

In Appendix C, a series of formulas are built to check Formula (21).

Based on Figure 2, Formula (21) can be converted into Formula (C.1).

$$\begin{aligned}\overrightarrow{OP} = {} & \frac{(\theta_2' - \theta) \times (\varphi_2' - \varphi)}{(\theta_2' - \theta_1') \times (\varphi_2' - \varphi_1')}(R + h_1', \theta_1', \varphi_1') \\ & + \frac{(\theta - \theta_1') \times (\varphi_2' - \varphi)}{(\theta_2' - \theta_1') \times (\varphi_2' - \varphi_1')}(R + h_2', \theta_2', \varphi_1') \\ & + \frac{(\theta_2' - \theta) \times (\varphi - \varphi_1')}{(\theta_2' - \theta_1') \times (\varphi_2' - \varphi_1')}(R + h_3', \theta_1', \varphi_2') \\ & + \frac{(\theta - \theta_1') \times (\varphi - \varphi_1')}{(\theta_2' - \theta_1') \times (\varphi_2' - \varphi_1')}(R + h_4', \theta_2', \varphi_2'),\end{aligned} \tag{C.1}$$

where $\theta_2' - \theta_1' > 0$ and $\varphi_2' - \varphi_1' > 0$.

Based on Formula (C.1), the radial distance P_ρ can be calculated by Formula (C.2).

$$\begin{aligned}P_\rho = {} & \frac{(\theta_2' - \theta) \times (\varphi_2' - \varphi)}{(\theta_2' - \theta_1') \times (\varphi_2' - \varphi_1')}(R + h_1') \\ & + \frac{(\theta - \theta_1') \times (\varphi_2' - \varphi)}{(\theta_2' - \theta_1') \times (\varphi_2' - \varphi_1')}(R + h_2') \\ & + \frac{(\theta_2' - \theta) \times (\varphi - \varphi_1')}{(\theta_2' - \theta_1') \times (\varphi_2' - \varphi_1')}(R + h_3') \\ & + \frac{(\theta - \theta_1') \times (\varphi - \varphi_1')}{(\theta_2' - \theta_1') \times (\varphi_2' - \varphi_1')}(R + h_4').\end{aligned} \tag{C.2}$$

Formula (C.2) can be simplified into Formulas (C.3), (C.4), (C.5), (C.6), (C.7) in a step-by-step process and converted into Formula (C.8) as a result.

$$\begin{aligned}P_\rho = {} & R \times \left[\frac{(\theta_2' - \theta) \times (\varphi_2' - \varphi)}{(\theta_2' - \theta_1') \times (\varphi_2' - \varphi_1')} + \frac{(\theta - \theta_1') \times (\varphi_2' - \varphi)}{(\theta_2' - \theta_1') \times (\varphi_2' - \varphi_1')} + \frac{(\theta_2' - \theta) \times (\varphi - \varphi_1')}{(\theta_2' - \theta_1') \times (\varphi_2' - \varphi_1')} + \frac{(\theta - \theta_1') \times (\varphi - \varphi_1')}{(\theta_2' - \theta_1') \times (\varphi_2' - \varphi_1')} \right] \\ & + \frac{(\theta_2' - \theta) \times (\varphi_2' - \varphi)}{(\theta_2' - \theta_1') \times (\varphi_2' - \varphi_1')} \times h_1' + \frac{(\theta - \theta_1') \times (\varphi_2' - \varphi)}{(\theta_2' - \theta_1') \times (\varphi_2' - \varphi_1')} \times h_2' + \frac{(\theta_2' - \theta) \times (\varphi - \varphi_1')}{(\theta_2' - \theta_1') \times (\varphi_2' - \varphi_1')} \times h_3' + \frac{(\theta - \theta_1') \times (\varphi - \varphi_1')}{(\theta_2' - \theta_1') \times (\varphi_2' - \varphi_1')} \times h_4',\end{aligned} \tag{C.3}$$

$$\begin{aligned}P_\rho = {} & R \times \frac{(\theta_2' - \theta) \times (\varphi_2' - \varphi) + (\theta - \theta_1') \times (\varphi_2' - \varphi) + (\theta_2' - \theta) \times (\varphi - \varphi_1') + (\theta - \theta_1') \times (\varphi - \varphi_1')}{(\theta_2' - \theta_1') \times (\varphi_2' - \varphi_1')} \\ & + \frac{(\theta_2' - \theta) \times (\varphi_2' - \varphi)}{(\theta_2' - \theta_1') \times (\varphi_2' - \varphi_1')} \times h_1' + \frac{(\theta - \theta_1') \times (\varphi_2' - \varphi)}{(\theta_2' - \theta_1') \times (\varphi_2' - \varphi_1')} \times h_2' + \frac{(\theta_2' - \theta) \times (\varphi - \varphi_1')}{(\theta_2' - \theta_1') \times (\varphi_2' - \varphi_1')} \times h_3' \\ & + \frac{(\theta - \theta_1') \times (\varphi - \varphi_1')}{(\theta_2' - \theta_1') \times (\varphi_2' - \varphi_1')} \times h_4',\end{aligned} \tag{C.4}$$

$$\begin{aligned}P_\rho = {} & R \times \frac{(\theta_2' - \theta) \times (\varphi_2' - \varphi + \varphi - \varphi_1') + (\theta - \theta_1') \times (\varphi_2' - \varphi + \varphi - \varphi_1')}{(\theta_2' - \theta_1') \times (\varphi_2' - \varphi_1')} + \frac{(\theta_2' - \theta) \times (\varphi_2' - \varphi)}{(\theta_2' - \theta_1') \times (\varphi_2' - \varphi_1')} \times h_1' \\ & + \frac{(\theta - \theta_1') \times (\varphi_2' - \varphi)}{(\theta_2' - \theta_1') \times (\varphi_2' - \varphi_1')} \times h_2' + \frac{(\theta_2' - \theta) \times (\varphi - \varphi_1')}{(\theta_2' - \theta_1') \times (\varphi_2' - \varphi_1')} \times h_3' + \frac{(\theta - \theta_1') \times (\varphi - \varphi_1')}{(\theta_2' - \theta_1') \times (\varphi_2' - \varphi_1')} \times h_4',\end{aligned} \tag{C.5}$$

$$P_\rho = R \times \frac{(\varphi_2' - \varphi_1') \times (\theta_2' - \theta + \theta - \theta_1')}{(\theta_2' - \theta_1') \times (\varphi_2' - \varphi_1')} + \frac{(\theta_2' - \theta) \times (\varphi_2' - \varphi)}{(\theta_2' - \theta_1') \times (\varphi_2' - \varphi_1')} \times h_1' + \frac{(\theta - \theta_1') \times (\varphi_2' - \varphi)}{(\theta_2' - \theta_1') \times (\varphi_2' - \varphi_1')} \times h_2' + \frac{(\theta_2' - \theta) \times (\varphi - \varphi_1')}{(\theta_2' - \theta_1') \times (\varphi_2' - \varphi_1')} \times h_3' + \frac{(\theta - \theta_1') \times (\varphi - \varphi_1')}{(\theta_2' - \theta_1') \times (\varphi_2' - \varphi_1')} \times h_4', \tag{C.6}$$

$$P_\rho = R \times \frac{(\theta_2' - \theta_1') \times (\varphi_2' - \varphi_1')}{(\theta_2' - \theta_1') \times (\varphi_2' - \varphi_1')} + \frac{(\theta_2' - \theta) \times (\varphi_2' - \varphi)}{(\theta_2' - \theta_1') \times (\varphi_2' - \varphi_1')} \times h_1' + \frac{(\theta - \theta_1') \times (\varphi_2' - \varphi)}{(\theta_2' - \theta_1') \times (\varphi_2' - \varphi_1')} \times h_2' + \frac{(\theta_2' - \theta) \times (\varphi - \varphi_1')}{(\theta_2' - \theta_1') \times (\varphi_2' - \varphi_1')} \times h_3' + \frac{(\theta - \theta_1') \times (\varphi - \varphi_1')}{(\theta_2' - \theta_1') \times (\varphi_2' - \varphi_1')} \times h_4', \tag{C.7}$$

$$P_\rho = R + \frac{(\theta_2' - \theta) \times (\varphi_2' - \varphi)}{(\theta_2' - \theta_1') \times (\varphi_2' - \varphi_1')} \times h_1' + \frac{(\theta - \theta_1') \times (\varphi_2' - \varphi)}{(\theta_2' - \theta_1') \times (\varphi_2' - \varphi_1')} \times h_2' + \frac{(\theta_2' - \theta) \times (\varphi - \varphi_1')}{(\theta_2' - \theta_1') \times (\varphi_2' - \varphi_1')} \times h_3' + \frac{(\theta - \theta_1') \times (\varphi - \varphi_1')}{(\theta_2' - \theta_1') \times (\varphi_2' - \varphi_1')} \times h_4'. \tag{C.8}$$

Based on Formula (C.1), the polar angle P_θ can be calculated by Formula (C.9).

$$P_\theta = \frac{(\theta_2' - \theta) \times (\varphi_2' - \varphi)}{(\theta_2' - \theta_1') \times (\varphi_2' - \varphi_1')} \times \theta_1' + \frac{(\theta - \theta_1') \times (\varphi_2' - \varphi)}{(\theta_2' - \theta_1') \times (\varphi_2' - \varphi_1')} \times \theta_2' + \frac{(\theta_2' - \theta) \times (\varphi - \varphi_1')}{(\theta_2' - \theta_1') \times (\varphi_2' - \varphi_1')} \times \theta_1' + \frac{(\theta - \theta_1') \times (\varphi - \varphi_1')}{(\theta_2' - \theta_1') \times (\varphi_2' - \varphi_1')} \times \theta_2'. \tag{C.9}$$

Formula (C.9) can be simplified into Formulas (C.10), (C.11), (C.12), (C.13), (C.14) in a step-by-step process and converted into Formula (C.15) as a result.

$$P_\theta = \frac{(\theta_2' - \theta) \times (\varphi_2' - \varphi) \times \theta_1' + (\theta - \theta_1') \times (\varphi_2' - \varphi) \times \theta_2' + (\theta_2' - \theta) \times (\varphi - \varphi_1') \times \theta_1' + (\theta - \theta_1') \times (\varphi - \varphi_1') \times \theta_2'}{(\theta_2' - \theta_1') \times (\varphi_2' - \varphi_1')}, \tag{C.10}$$

$$P_\theta = \frac{\theta_1' \times (\theta_2' - \theta) \times (\varphi_2' - \varphi + \varphi - \varphi_1') + \theta_2' \times (\theta - \theta_1') \times (\varphi_2' - \varphi + \varphi - \varphi_1')}{(\theta_2' - \theta_1') \times (\varphi_2' - \varphi_1')}, \tag{C.11}$$

$$P_\theta = \frac{(\varphi_2' - \varphi_1') \times [\theta_1' \times (\theta_2' - \theta) + \theta_2' \times (\theta - \theta_1')]}{(\theta_2' - \theta_1') \times (\varphi_2' - \varphi_1')}, \tag{C.12}$$

$$P_\theta = \frac{(\varphi_2' - \varphi_1') \times (\theta_1' \times \theta_2' - \theta_1' \times \theta + \theta_2' \times \theta - \theta_2' \times \theta_1')}{(\theta_2' - \theta_1') \times (\varphi_2' - \varphi_1')}, \tag{C.13}$$

$$P_\theta = \frac{(\varphi_2' - \varphi_1') \times (\theta_2' - \theta_1') \times \theta}{(\theta_2' - \theta_1') \times (\varphi_2' - \varphi_1')}, \tag{C.14}$$

$$P_\theta = \theta. \tag{C.15}$$

Based on Formula (C.1), the azimuthal angle P_φ can be calculated by Formula (C.16).

$$P_\varphi = \frac{(\theta_2' - \theta) \times (\varphi_2' - \varphi)}{(\theta_2' - \theta_1') \times (\varphi_2' - \varphi_1')} \times \varphi_1' + \frac{(\theta - \theta_1') \times (\varphi_2' - \varphi)}{(\theta_2' - \theta_1') \times (\varphi_2' - \varphi_1')} \times \varphi_1' + \frac{(\theta_2' - \theta) \times (\varphi - \varphi_1')}{(\theta_2' - \theta_1') \times (\varphi_2' - \varphi_1')} \times \varphi_2' + \frac{(\theta - \theta_1') \times (\varphi - \varphi_1')}{(\theta_2' - \theta_1') \times (\varphi_2' - \varphi_1')} \times \varphi_2'. \tag{C.16}$$

Formula (C.16) can be simplified into Formulas (C.17), (C.18), (C.19), (C.20), (C.21) in a step-by-step process and converted into Formula (C.22) as a result.

$$P_\varphi = \frac{(\theta_2' - \theta) \times (\varphi_2' - \varphi) \times \varphi_1' + (\theta - \theta_1') \times (\varphi_2' - \varphi) \times \varphi_1' + (\theta_2' - \theta) \times (\varphi - \varphi_1') \times \varphi_2' + (\theta - \theta_1') \times (\varphi - \varphi_1') \times \varphi_2'}{(\theta_2' - \theta_1') \times (\varphi_2' - \varphi_1')}, \tag{C.17}$$

$$P_\varphi = \frac{\varphi_1' \times (\varphi_2' - \varphi) \times (\theta_2' - \theta + \theta - \theta_1') + \varphi_2' \times (\varphi - \varphi_1') \times (\theta_2' - \theta + \theta - \theta_1')}{(\theta_2' - \theta_1') \times (\varphi_2' - \varphi_1')}, \tag{C.18}$$

$$P_\varphi = \frac{(\theta_2' - \theta_1') \times [\varphi_1' \times (\varphi_2' - \varphi) + \varphi_2' \times (\varphi - \varphi_1')]}{(\theta_2' - \theta_1') \times (\varphi_2' - \varphi_1')}, \tag{C.19}$$

$$P_\varphi = \frac{(\theta_2' - \theta_1') \times (\varphi_1' \times \varphi_2' - \varphi_1' \times \varphi + \varphi_2' \times \varphi - \varphi_2' \times \varphi_1')}{(\theta_2' - \theta_1') \times (\varphi_2' - \varphi_1')}, \tag{C.20}$$

$$P_\varphi = \frac{(\theta_2' - \theta_1') \times (\varphi_2' - \varphi_1') \times \varphi}{(\theta_2' - \theta_1') \times (\varphi_2' - \varphi_1')}, \tag{C.21}$$

$$P_\varphi = \varphi. \tag{C.22}$$

Based on Formulas (C.8), (C.15), (C.22), Formula (C.1) can be converted into Formula (C.23).

$$\begin{aligned}\overrightarrow{OP} = \Bigg(& R + \frac{(\theta_2' - \theta) \times (\varphi_2' - \varphi)}{(\theta_2' - \theta_1') \times (\varphi_2' - \varphi_1')} \times h_1' \\ & + \frac{(\theta - \theta_1') \times (\varphi_2' - \varphi)}{(\theta_2' - \theta_1') \times (\varphi_2' - \varphi_1')} \times h_2' \\ & + \frac{(\theta_2' - \theta) \times (\varphi - \varphi_1')}{(\theta_2' - \theta_1') \times (\varphi_2' - \varphi_1')} \times h_3' \\ & + \frac{(\theta - \theta_1') \times (\varphi - \varphi_1')}{(\theta_2' - \theta_1') \times (\varphi_2' - \varphi_1')} \times h_4', \theta, \varphi \Bigg).\end{aligned} \tag{C.23}$$

Compare Formula (C.23) with the origin coordinate $P(R + h, \theta, \varphi)$, the equational relations can be expressed by Formula (C.24).

$$\begin{aligned} & R + \frac{(\theta_2' - \theta) \times (\varphi_2' - \varphi)}{(\theta_2' - \theta_1') \times (\varphi_2' - \varphi_1')} \times h_1' \\ & + \frac{(\theta - \theta_1') \times (\varphi_2' - \varphi)}{(\theta_2' - \theta_1') \times (\varphi_2' - \varphi_1')} \times h_2' \\ & + \frac{(\theta_2' - \theta) \times (\varphi - \varphi_1')}{(\theta_2' - \theta_1') \times (\varphi_2' - \varphi_1')} \times h_3' \\ & + \frac{(\theta - \theta_1') \times (\varphi - \varphi_1')}{(\theta_2' - \theta_1') \times (\varphi_2' - \varphi_1')} \times h_4' = R + h, \\ & \theta = \theta, \\ & \varphi = \varphi. \end{aligned} \tag{C.24}$$

As a result, Formula (20) is available after checking and h can be calculated by Formula (21) on the basis of Formula (C.24).

D. Derivation Process of Table 2

In Appendix D, a series of formulas are built to work out Table 2. It is worth noting that all the θ and φ in degree measure should be converted into radian measure by multiplying $\pi/180^\circ$ before calculating.

Now, we calculate the movements.

Based on Formulas (7), (12), (21), the vehicle movement $\overrightarrow{P_1P_2}$ under Direct Solution, Original Model, MDE Model can be calculated respectively by Formulas (29), (30), (31).

$$\begin{aligned} D^2 = & \Bigg[(6378137.00 + 145) \times \sin\left(109.4983^\circ \times \frac{\pi}{180^\circ}\right) \\ & \times \cos\left(18.2274^\circ \times \frac{\pi}{180^\circ}\right) - (6378137.00 + 147) \\ & \times \sin\left(109.4987^\circ \times \frac{\pi}{180^\circ}\right) \times \cos\left(18.2272^\circ \times \frac{\pi}{180^\circ}\right) \Bigg]^2 \\ & + \Bigg[(6378137.00 + 145) \times \sin\left(109.4983^\circ \times \frac{\pi}{180^\circ}\right) \\ & \times \sin\left(18.2274^\circ \times \frac{\pi}{180^\circ}\right) - (6378137.00 + 147) \\ & \times \sin\left(109.4987^\circ \times \frac{\pi}{180^\circ}\right) \times \sin\left(18.2272^\circ \times \frac{\pi}{180^\circ}\right) \Bigg]^2 \\ & + \Bigg[(6378137.00 + 145) \times \cos\left(109.4983^\circ \times \frac{\pi}{180^\circ}\right) \\ & - (6378137.00 + 147) \times \cos\left(109.4987^\circ \times \frac{\pi}{180^\circ}\right) \Bigg]^2, \end{aligned} \tag{D.1}$$

$$\begin{aligned} d = & 6378137.00 \times \arccos\Bigg(\sin\left(109.4983^\circ \times \frac{\pi}{180^\circ}\right) \\ & \times \sin\left(109.4987^\circ \times \frac{\pi}{180^\circ}\right) \times \cos\left(\left(18.2272^\circ \times \frac{\pi}{180^\circ}\right) \right. \\ & \left. - \left(18.2274^\circ \times \frac{\pi}{180^\circ}\right)\right) + \cos\left(109.4983^\circ \times \frac{\pi}{180^\circ}\right) \\ & \times \cos\left(109.4987^\circ \times \frac{\pi}{180^\circ}\right)\Bigg), \end{aligned} \tag{D.2}$$

$$\begin{aligned} d'^2 = & \Bigg[\left(6378137.00 + \frac{145 + 147}{2}\right) \times \arccos \\ & \cdot \Bigg(\sin\left(109.4983^\circ \times \frac{\pi}{180^\circ}\right) \times \sin\left(109.4987^\circ \times \frac{\pi}{180^\circ}\right) \\ & \times \cos\left(\left(18.2272^\circ \times \frac{\pi}{180^\circ}\right) - \left(18.2274^\circ \times \frac{\pi}{180^\circ}\right)\right) \\ & + \cos\left(109.4983^\circ \times \frac{\pi}{180^\circ}\right) \\ & \times \cos\left(109.4987^\circ \times \frac{\pi}{180^\circ}\right)\Bigg)\Bigg]^2 + (145 - 147)^2. \end{aligned} \tag{D.3}$$

Based on Formulas (D.1), (D.2), (D.3), the values of D, d, d' are certain as shown by Formula (D.4).

$$\begin{aligned} D &= 49.267562, \\ d &= 49.225885, \\ d' &= 49.267623. \end{aligned} \tag{D.4}$$

Now, Spherical Bilinear Interpolation Model is adopted. Based on Formula (17), h_1 can be calculated by Formulas (D.5).

$$\begin{aligned} h_1 = & \frac{(109.499^\circ - 109.4983^\circ) \times (18.228^\circ - 18.2274^\circ)}{(109.499^\circ - 109.498^\circ) \times (18.228^\circ - 18.227^\circ)} \times 149.72 \\ & + \frac{(109.4983^\circ - 109.498^\circ) \times (18.228^\circ - 18.2274^\circ)}{(109.499^\circ - 109.498^\circ) \times (18.228^\circ - 18.227^\circ)} \times 150.81 \\ & + \frac{(109.499^\circ - 109.4983^\circ) \times (18.2274^\circ - 18.227^\circ)}{(109.499^\circ - 109.498^\circ) \times (18.228^\circ - 18.227^\circ)} \times 139.55 \\ & + \frac{(109.4983^\circ - 109.498^\circ) \times (18.2274^\circ - 18.227^\circ)}{(109.499^\circ - 109.498^\circ) \times (18.228^\circ - 18.227^\circ)} \times 132.45. \end{aligned} \tag{D.5}$$

Formula (D.5) can be simplified into Formulas (D.6) and converted into Formula (D.7) as a result.

$$\begin{aligned} h_1 = & 0.7 \times 0.6 \times 149.72 + 0.3 \times 0.6 \times 150.81 \\ & + 0.7 \times 0.4 \times 139.55 + 0.3 \times 0.4 \times 132.45, \end{aligned} \tag{D.6}$$

$$h_1 = 144.9962 \approx 145.00\,(m). \tag{D.7}$$

Based on Formula (17), h_2 can be calculated by Formula (D.8).

$$\begin{aligned} h_2 = & \frac{(109.499^\circ - 109.4987^\circ) \times (18.228^\circ - 18.2272^\circ)}{(109.499^\circ - 109.498^\circ) \times (18.228^\circ - 18.227^\circ)} \times 149.72 \\ & + \frac{(109.4987^\circ - 109.498^\circ) \times (18.228^\circ - 18.2272^\circ)}{(109.499^\circ - 109.498^\circ) \times (18.228^\circ - 18.227^\circ)} \times 150.81 \\ & + \frac{(109.499^\circ - 109.4987^\circ) \times (18.2272^\circ - 18.227^\circ)}{(109.499^\circ - 109.498^\circ) \times (18.228^\circ - 18.227^\circ)} \times 139.55 \\ & + \frac{(109.4987^\circ - 109.498^\circ) \times (18.2272^\circ - 18.227^\circ)}{(109.499^\circ - 109.498^\circ) \times (18.228^\circ - 18.227^\circ)} \times 132.45. \end{aligned} \tag{D.8}$$

Formula (D.8) can be simplified into Formulas (D.9) and converted into Formula (D.10) as a result.

$$h_2 = 0.3 \times 0.8 \times 149.72 + 0.7 \times 0.8 \times 150.81 + 0.3 \times 0.2 \times 139.55 + 0.7 \times 0.2 \times 132.45, \tag{D.9}$$

$$h_2 = 147.3024 \approx 147.30\,(m). \tag{D.10}$$

Based on Formula (D.7), (D.10), the coordinates of points $P_1(R + 145.00, 109.4983^\circ, 18.2274^\circ)$, $P_2(R + 147.30, 109.4987^\circ, 18.2272^\circ)$ are certain.

Now, we calculate the movements.

Based on Formula (7), (12), (21), the vehicle movement $\overrightarrow{P_1P_2}$ under Direct Solution, Original Model, MDE Model can be calculated respectively by Formula (D.11), (D.12), (D.13).

$$\begin{aligned} D^2 = {} & \left[(6378137.00 + 145.00) \times \sin\left(109.4983^\circ \times \frac{\pi}{180^\circ}\right) \times \cos\left(18.2274^\circ \times \frac{\pi}{180^\circ}\right) - (6378137.00 + 147.30) \times \sin\left(109.4987^\circ \times \frac{\pi}{180^\circ}\right) \times \cos\left(18.2272^\circ \times \frac{\pi}{180^\circ}\right)\right]^2 \\ & + \left[(6378137.00 + 145.00) \times \sin\left(109.4983^\circ \times \frac{\pi}{180^\circ}\right) \times \sin\left(18.2274^\circ \times \frac{\pi}{180^\circ}\right) - (6378137.00 + 147.30) \times \sin\left(109.4987^\circ \times \frac{\pi}{180^\circ}\right) \times \sin\left(18.2272^\circ \times \frac{\pi}{180^\circ}\right)\right]^2 \\ & + \left[(6378137.00 + 145.00) \times \cos\left(109.4983^\circ \times \frac{\pi}{180^\circ}\right) - (6378137.00 + 147.30) \times \cos\left(109.4987^\circ \times \frac{\pi}{180^\circ}\right)\right]^2, \end{aligned} \tag{D.11}$$

$$\begin{aligned} d = {} & 6378137.00 \times \arccos\left(\sin\left(109.4983^\circ \times \frac{\pi}{180^\circ}\right) \times \sin\left(109.4987^\circ \times \frac{\pi}{180^\circ}\right) \times \cos\left(\left(18.2272^\circ \times \frac{\pi}{180^\circ}\right) - \left(18.2274^\circ \times \frac{\pi}{180^\circ}\right)\right) + \cos\left(109.4983^\circ \times \frac{\pi}{180^\circ}\right) \times \cos\left(109.4987^\circ \times \frac{\pi}{180^\circ}\right)\right), \end{aligned} \tag{D.12}$$

$$\begin{aligned} d'^2 = {} & \left[\left(6378137.00 + \frac{145.00 + 147.30}{2}\right) \times \arccos \cdot \left(\sin\left(109.4983^\circ \times \frac{\pi}{180^\circ}\right) \times \sin\left(109.4987^\circ \times \frac{\pi}{180^\circ}\right) \times \cos\left(\left(18.2272^\circ \times \frac{\pi}{180^\circ}\right) - \left(18.2274^\circ \times \frac{\pi}{180^\circ}\right)\right) + \cos\left(109.4983^\circ \times \frac{\pi}{180^\circ}\right) \times \cos\left(109.4987^\circ \times \frac{\pi}{180^\circ}\right)\right)\right]^2 \\ & + (145.00 - 147.30)^2, \end{aligned} \tag{D.13}$$

Based on Formulas (D.11), (D.12), (D.13), the values of D, d, d' are certain as shown by Formula (D.14).

$$\begin{aligned} D &= 49.280653, \\ d &= 49.225885, \\ d' &= 49.280715. \end{aligned} \tag{D.14}$$

Based on Formulas (D.4), (D.14), Table 2 was worked out as a result.

Data Availability

The data collected during the study were freely available at the website. https://transportdata.cn/traffictravel/open. In detail, the data of Liaoyang was freely available at the website https://transportdata.cn/traffictravel/open/detail?id=180, the data of Zhengzhou was freely available at the website https://transportdata.cn/traffictravel/open/detail?id=205, the data of Sanya was freely available at the website https://transportdata.cn/traffictravel/open/detail?id=188.

Conflicts of Interest

The authors declare that there are no conflicts of interest regarding the publication of this article.

Authors' Contributions

Jiawei Gui contributed to conceptualization, methodology, software, validation, formal analysis, investigation, resources, data curation, manuscript preparation for all versions, and funding acquisition in part. Qunqi Wu contributed to funding acquisition in part and project administration. The authors reviewed the results and approved the final version of the manuscript.

Acknowledgments

The authors are indebted to the Kamal D. Singh and anonymous referees for their thoughtful comments that have helped substantially improve this work. The authors are also indebted to Ramya Kabali, Pani Vignesh, and anonymous editors for providing excellent editing services. Jiawei Gui was rewarded by the National Scholarship of China for doctoral students and appreciated that. The work described in this article was supported in part by the Strategic Planning Research Project of Ministry of Transport of China [2018-7-9] and [2018-16-9], in part by the National Social Science Fund of China [17BJY139], in part by the Chang'an University Excellent Doctoral Dissertation Project of Chinese Universities Scientific Fund of China [300102239718].

Supplementary Materials

In this section, a file named "Data.xlsx" is presented. In this file, it recorded the major data used in this study,

including Sample, Direct Solution, Original Model, MDE Model and the comparison results between them. Due to space limitation, tables in this file (819 KB in size) records only partial contents of full data (over 500 MB in size). (*Supplementary Materials*)

References

[1] K. Piamrat, A. Ksentini, J.-M. Bonnin, and C. Viho, "Radio resource management in emerging heterogeneous wireless networks," *Computer Communications*, vol. 34, no. 9, pp. 1066–1076, 2011.

[2] L. Atzori, A. Iera, and G. Morabito, "The internet of things: a survey," *Computer Networks*, vol. 54, no. 15, pp. 2787–2805, 2010.

[3] D. Miorandi, S. Sicari, F. De Pellegrini, and I. Chlamtac, "Internet of things: vision, applications and research challenges," *Ad Hoc Networks*, vol. 10, no. 7, pp. 1497–1516, 2012.

[4] L. D. Xu, W. He, and S. C. Li, "Internet of things in industries: a survey," *IEEE Transactions on Industrial Informatics*, vol. 10, no. 4, pp. 2233–2243, 2014.

[5] A. Zanella, N. Bui, A. Castellani, L. Vangelista, and M. Zorzi, "Internet of things for smart cities," *IEEE Internet of Things Journal*, vol. 1, no. 1, pp. 22–32, 2014.

[6] F. Y. Wang, "Parallel control and management for intelligent transportation systems: concepts, architectures, and applications," *IEEE Transactions on Intelligent Transportation Systems*, vol. 11, no. 3, pp. 630–638, 2010.

[7] O. Kaiwartya, A. H. Abdullah, Y. Cao, M. Prasad, C.-T. Lin, and X. Liu, "Internet of vehicles : motivation, layered architecture, network model, challenges, and future aspects," *IEEE Access*, vol. 4, pp. 5356–5373, 2016.

[8] N. Lu, N. Cheng, N. Zhang, X. Shen, and J. W. Mark, "Connected vehicles: solutions and challenges," *IEEE Internet of Things Journal*, vol. 1, no. 4, pp. 289–299, 2014.

[9] F. Yang, S. Wang, J. Li, Z. Liu, and Q. Sun, "An overview of internet of vehicles," *China Communications*, vol. 11, no. 10, pp. 1–15, 2014.

[10] P. Rawat, K. D. Singh, and J. M. Bonnin, "Cognitive radio for M2M and internet of things: a Survey," *Computer Communications*, vol. 94, pp. 1–29, 2016.

[11] K. D. Singh, P. Rawat, and J. M. Bonnin, "Cognitive radio for vehicular ad Hoc networks (CR-VANETs): approaches and challenges," *EURASIP Journal on Wireless Communications and Networking*, vol. 49, no. 1, pp. 1–22, 2014.

[12] H. C. Chen, "TCABRP: a trust-based cooperation authentication bit-map routing protocol against insider security threats in wireless ad hoc networks," *IEEE Systems Journal*, vol. 11, no. 2, pp. 449–459, 2017.

[13] X. M. Huang, R. Yu, M. Pan, and L. Shu, "Secure roadside unit hotspot against eavesdropping based traffic analysis in edge computing based internet of vehicles," *IEEE Access*, vol. 6, pp. 62371–62383, 2018.

[14] T. A. Butt, R. Iqbal, S. C. Shah, and T. Umar, "Social internet of vehicles: architecture and enabling technologies," *Computers & Electrical Engineering*, vol. 69, pp. 68–84, 2018.

[15] M. Chen, Y. Tian, G. Fortino, J. Zhang, and I. Humar, "Cognitive internet of vehicles," *Computer Communications*, vol. 120, pp. 58–70, 2018.

[16] H. Hartenstein and K. P. Laberteaux, "A tutorial survey on vehicular ad hoc networks," *IEEE Communications Magazine*, vol. 46, no. 6, pp. 164–171, 2008.

[17] S. Al-Sultan, M. M. Al-Doori, A. H. Al-Bayatti, and H. Zedan, "A comprehensive survey on vehicular ad hoc network," *Journal of Network and Computer Applications*, vol. 37, pp. 380–392, 2014.

[18] M. Chaqfeh, A. Lakas, and I. Jawhar, "A survey on data dissemination in vehicular ad hoc networks," *Vehicular Communications*, vol. 1, no. 4, pp. 214–225, 2014.

[19] A. Petrovskaya and S. Thrun, "Model based vehicle detection and tracking for autonomous urban driving," *Autonomous Robots*, vol. 26, no. 2–3, pp. 123–139, 2009.

[20] S. E. Shladover, C. A. Desoer, J. K. Hedrick et al., "Automatic vehicle control developments in the PATH program," *IEEE Transactions on Vehicular Technology*, vol. 40, no. 1, pp. 114–130, 1991.

[21] T. Luettel, M. Himmelsbach, and H. J. Wuensche, "Autonomous ground vehicles-concepts and a path to the future," *Proceedings of the IEEE*, vol. 100, pp. 1831–1839, 2012.

[22] P. Koopman and M. Wagner, "Autonomous vehicle safety: an interdisciplinary challenge," *IEEE Intelligent Transportation Systems Magazine*, vol. 9, no. 1, pp. 90–96, 2017.

[23] H. W. Wang, F. You, X. N. Chu, X. Li, and X. Sun, "Research on customer marketing acceptance for future automatic driving-a case study in china city," *IEEE Access*, vol. 7, pp. 20938–20949, 2019.

[24] H.-C. Chen, I. You, C.-E. Weng, C.-H. Cheng, and Y.-F. Huang, "A security gateway application for end-to-end M2M communications," *Computer Standards & Interfaces*, vol. 44, pp. 85–93, 2016.

[25] H. Park, C. Lee, Y. S. Lee, and E.-J. Kim, "Performance analysis for contention adaptation of M2M devices with directional antennas," *Journal of Supercomputing*, vol. 72, no. 9, pp. 3387–3408, 2016.

[26] H. Park and E. J. Kim, "Location-oriented multiplexing transmission for capillary machine-to-machine systems," *Multimedia Tools and Applications*, vol. 75, no. 22, pp. 14707–14719, 2016.

[27] S. U. Rehman, M. A. Khan, M. Imran, T. A. Zia, and M. Iftikhar, "Enhancing quality-of-service conditions using a cross-layer paradigm for ad-hoc vehicular communication," *IEEE Access*, vol. 5, pp. 12404–12416, 2017.

[28] B. Fan, H. Tian, S. Zhu, Y. Chen, and X. Zhu, "Traffic-aware relay vehicle selection in millimeter-wave vehicle-to-vehicle communication," *IEEE Wireless Communications Letters*, vol. 8, no. 2, pp. 400–403, 2019.

[29] N. Lyamin, D. Kleyko, Q. Delooz, and A. Vinel, "Real-time jamming DoS detection in safety-critical V2V C-ITS using data mining," *IEEE Communications Letters*, vol. 23, no. 3, pp. 442–445, 2019.

[30] E. Han, H. P. Lee, S. Park, J. So, and I. Yun, "Optimal signal control algorithm for signalized intersections under a V2I communication environment," *Journal of Advanced Transportation*, vol. 2019, Article ID 6039741, 9 pages, 2019.

[31] D. Jia, D. Ngoduy, and H. L. Vu, "A multiclass microscopic model for heterogeneous platoon with vehicle-to-vehicle communication," *Transportmetrica B-Transport Dynamics*, vol. 7, no. 1, pp. 448–472, 2019.

[32] Y. Lecun, Y. Bengio, and G. Hinton, "Deep learning," *Nature*, vol. 521, no. 7553, pp. 436–444, 2015.

[33] M. Aramrattana, T. Larsson, J. Jansson, and A. Nåbo, "A simulation framework for cooperative intelligent transport

systems testing and evaluation," *Transportation Research Part F-Traffic Psychology and Behaviour*, vol. 61, pp. 268–280, 2019.

[34] M. Elwekeil, T. Wang, and S. Zhang, "Deep learning for joint adaptations of transmission rate and payload length in vehicular networks," *Sensors*, vol. 19, no. 5, p. 1113, 2019.

[35] C. Lv, X. Hu, A. Sangiovanni-Vincentelli, Y. Li, C. M. Martinez, and D. Cao, "Driving-style-based codesign optimization of an automated electric vehicle: a cyber-physical system approach," *IEEE Transactions on Industrial Electronics*, vol. 66, no. 4, pp. 2965–2975, 2019.

[36] J. Li, G. Luo, N. Cheng et al., "An end-to-end load balancer based on deep learning for vehicular network traffic control," *IEEE Internet of Things Journal*, vol. 6, no. 1, pp. 953–966, 2019.

[37] J. Zhang, F.-Y. Wang, K. Wang, W.-H. Lin, X. Xu, and C. Chen, "Data-driven intelligent transportation systems: a survey," *IEEE Transactions on Intelligent Transportation Systems*, vol. 12, no. 4, pp. 1624–1639, 2011.

[38] F. Frankel and R. Reid, "Big data: distilling meaning from data," *Nature*, vol. 455, no. 7209, p. 30, 2008.

[39] W. Los and J. Wood, "Dealing with data: upgrading infrastructure," *Science*, vol. 331, no. 6024, pp. 1515–1516, 2011.

[40] J. Gubbi, R. Buyya, S. Marusic, and M. Palaniswami, "Internet of Things (IoT): a vision, architectural elements, and future directions," *Future Generation Computer Systems*, vol. 29, no. 7, pp. 1645–1660, 2013.

[41] M. Whaiduzzaman, M. Sookhak, A. Gani, and R. Buyya, "A survey on vehicular cloud computing," *Journal of Network and Computer Applications*, vol. 40, pp. 325–344, 2014.

[42] A. Al-Fuqaha, M. Guizani, M. Mohammadi, M. Aledhari, and M. Ayyash, "Internet of things: a survey on enabling technologies, protocols, and applications," *IEEE Communications Surveys and Tutorials*, vol. 17, no. 4, pp. 2347–2376, 2015.

[43] Z. L. Ning, J. Huang, and X. J. Wang, "Vehicular fog computing: enabling real-time traffic management for smart cities," *IEEE Wireless Communications*, vol. 26, no. 1, pp. 87–93, 2019.

[44] J. Tang, S. Zhang, X. Chen, F. Liu, and Y. Zou, "Taxi trips distribution modeling based on entropy-maximizing theory: a case study in Harbin City-China," *Physica A-Statistical Mechanics and Its Applications*, vol. 493, pp. 430–443, 2018.

[45] J. Tang, J. Liang, S. Zhang, H. Huang, and F. Liu, "Inferring driving trajectories based on probabilistic model from large scale taxi GPS data," *Physica A-Statistical Mechanics and Its Applications*, vol. 506, pp. 566–577, 2018.

[46] J. Bao, P. Liu, X. Qin, and H. Zhou, "Understanding the effects of trip patterns on spatially aggregated crashes with large-scale taxi GPS data," *Accident Analysis and Prevention*, vol. 120, pp. 281–294, 2018.

[47] P. Rawat, K. D. Singh, H. Chaouchi, and J. M. Bonnin, "Wireless sensor networks: a survey on recent developments and potential synergies," *Journal of Supercomputing*, vol. 68, no. 1, pp. 1–48, 2014.

[48] M. Gerla, E.-K. Lee, G. Pau, and U. Lee, "Internet of vehicles: from intelligent grid to autonomous cars and vehicular clouds," in *2014 IEEE World Forum on Internet of Things*, pp. 241–246, Seoul, South Korea, 2014.

[49] M. N. Rastgoo, B. Nakisa, A. Rakotonirainy, V. Chandran, and D. Tjondronegoro, "A critical review of proactive detection of driver stress levels based on multimodal measurements," *ACM Computing Surveys*, vol. 51, no. 5, pp. 35–35, 2019.

[50] S. Barua, M. U. Ahmed, C. Ahlstrom, and S. Begum, "Automatic driver sleepiness detection using EEG, EOG and contextual information," *Expert Systems with Applications*, vol. 115, pp. 121–135, 2019.

[51] M.-S. Chen, C.-P. Hwang, T.-Y. Ho et al., "Driving behaviors analysis based on feature selection and statistical approach: a preliminary study," *Journal of Supercomputing*, vol. 75, no. 4, pp. 2007–2026, 2019.

[52] A. M. El-Geneidy, J. Horning, and K. J. Krizek, "Analyzing transit service reliability using detailed data from automatic vehicular locator systems," *Journal of Advanced Transportation*, vol. 45, no. 1, pp. 66–79, 2011.

[53] Z. Ning, X. Hu, Z. Chen, and M. Zhou, B. Hu, J. Cheng, and M. S. Obaidat, "A cooperative quality-aware service access system for social internet of vehicles," *IEEE Internet of Things Journal*, vol. 5, no. 4, pp. 2506–2517, 2018.

[54] C. Yuan, D. Wu, D. Wei, and H. Liu, "Modeling and analyzing taxi congestion premium in congested cities," *Journal of Advanced Transportation*, vol. 2017, Article ID 2619810, 12 pages, 2017.

[55] J. Song, F. Chen, Q. Wu, W. Liu, F. Xue, and K. Du, "Optimization of passenger transportation corridor mode supply structure in regional comprehensive transport considering economic equilibrium," *Sustainability*, vol. 11, no. 4, pp. 1–18, 2019.

[56] W. Dou, W. Tang, S. Li, S. Yu, and K.-K. Raymond Choo, "A heuristic line piloting method to disclose malicious taxicab driver's privacy over GPS big data," *Information Sciences*, vol. 483, pp. 247–261, 2019.

[57] J. Tang, Y. Wang, W. Hao, F. Liu, H. Huang, and Y. Wang, "A mixed path size logit-based taxi customer-search model considering spatio-temporal factors in route choice," *IEEE Transactions on Intelligent Transportation Systems*, pp. 1–12, 2019.

[58] J. Gui and Q. Wu, "Taxi efficiency measurements based on motorcade-sharing model: evidence from GPS-equipped taxi data in Sanya," *Journal of Advanced Transportation*, vol. 2018, Article ID 4360516, 10 pages, 2018.